Parallel and non-parallel features of adaptive radiation in Yucatán pupfishes

Matthew C. Kustra[1,2,3,*], David Tian[1,2], M. Fernanda Palominos[1,2], Feifei Guo[1,2], Dylan Chau[1,2], Oskar Golwala[1,2], HoWan Chan[4], Andrés Alvarez Zapata[5], Reyna Guadalupe Cetz Paredes[5], Frida Ximena Cortés Sánchez[6], Sonia Gabriela Hernández[6], Adan Fernando Mar-Silva[6], Fernando Mex[7], Charles Tralka[1,2], Maribel Badillo-Alemán[7], Juan J. Schmitter-Soto[8], Carlos A. Gracida-Juárez[9], Christopher M. Martinez[10], Jairo Arroyave[6], and Christopher H. Martin[1,2]

[1]Department of Integrative Biology, University of California, Berkeley, CA, United States

[2]Museum of Vertebrate Zoology, University of California, Berkeley, CA, United States

[3]Miller Institute for Basic Research in Science, University of California, Berkeley, CA, United States

[4]Department of BioSciences, Rice University, Houston, TX, United States

[5]Instituto Tecnologico Superior de Conkal, Yucatan, Mexico

[6]Instituto de Biología, Universidad Nacional Autónoma de México, Mexico City, Mexico

[7]Unidad Multidisciplinaria de Docencia e Investigación, Unidad Sisal, Universidad Nacional Autónoma de México, Sisal, Yucatán, Mexico

[8] Departamento de Sistemática y Ecología Acuática, El Colegio de la Frontera Sur, Chetumal, Quintana Roo, Mexico

[9]Subdirección de Posgrado e Investigación, Tecnológico Nacional de México, Campus Felipe Carrillo Puerto.Carretera a Vigía Chico km 1.5, 77200 Felipe Carrillo Puerto, Quintana Roo.

[10]Department of Ecology and Evolutionary Biology, University of California, Irvine, CA, United States

*Corresponding author: matthewckustra@berkeley.edu

Abstract

Understanding the extent of parallelism across adaptive radiations remains a central problem in evolutionary biology. We used whole-genome resequencing of 123 individuals to compare an adaptive radiation of *Cyprinodon* pupfishes in Laguna Chichancanab, Mexico, to an independent radiation of San Salvador Island (SSI) pupfishes in the Bahamas, and assess the repeatability of adaptive genetic architecture, sources of adaptive variation, and stages of selection. Despite rapid craniofacial divergence of trophic specialists within 8-15 kya, only two candidate genes (3.6%) were shared between Caribbean radiations. Although adaptive introgression played a major role on SSI, we found minimal evidence of adaptive introgression in Chichancanab, likely due to geographic isolation of this inland lake. Instead, de novo mutations provided a substantial source of adaptive variation (30.6%) for the endemic zooplanktivore, 15.3 times higher than the endemic scale-eater on SSI. We found strong evidence that selection occurred in stages, first on regulatory and standing genetic variation, then on de novo and nonsynonymous mutations, parallel to SSI. We then verified that adaptive variants near vision-development and spermatogenesis genes, uniquely within Chichancanab, are consistent with greater visual acuity and divergent sperm morphology in the zoooplanktivore. Consistent with extensive adaptive de novo mutations in *WNT10A* and rapid diversification of tooth size in the zooplanktivore, we found that experimental inhibition of this pathway in generalists results in narrower teeth. We conclude that de novo mutations, not introgression, can drive rapid adaptive radiations in isolated environments.

Introduction

Much of biodiversity results from adaptive radiation—when a clade diversifies rapidly into three or more new species (1–5). Young adaptive radiations provide excellent systems for investigating speciation and adaptation (3, 6–9). However, it remains unclear to what degree radiations occur in parallel given similar starting positions on the adaptive landscape with similar levels of genetic diversity, gene flow, and ecological opportunity (10, 11).

Beneficial de novo mutations can provide novel variation to reach new fitness peaks on the adaptive landscape during adaptive radiation (12, 13); however, the longer times needed for de novo beneficial mutations to arise contradicts the short timescales of rapid divergence (11, 14, 15). Hybridization can introduce large amounts of genetic variation and novel phenotypes (transgressive segregation) through adaptive introgression and hybrid swarms, enabling populations to reach previously inaccessible fitness peaks (16). Support for an important role of hybridization in adaptive radiations has been demonstrated both theoretically (17, 18) and empirically in many systems (3, 19–27). However, we still do not know the relative importance of different sources of genetic variation for triggering and sustaining adaptive radiations across time and space.

Caribbean pupfishes are a remarkable system for assessing the repeatability of adaptive radiations due to two independent, recent adaptive radiations each containing a generalist and multiple trophic specialists within isolated lake environments that have historically lacked predatory fishes and most competitors except *Gambusia*. The San Salvador Island (SSI), Bahamas radiation proceeded predominantly via the reassembly of pre-existing standing genetic variation found throughout the Caribbean, with substantial contributions of adaptive introgression to both the molluscivore (durophage) and scale-eating (lepidophage) specialists.

Only 0% and 2% of adaptive mutations in the molluscivore and scale-eater, respectively, were de novo mutations unique to SSI (26, 28–32). However, it previously was unknown how a second radiation in Laguna Chichancanab, Mexico, drawing from the same Caribbean pool of standing genetic variation unfolded over the same timeframe.

Here, we use whole-genome resequencing of 123 individuals to provide insight into the genomic architecture and genetic origins of the Laguna Chichancanab *Cyprinodon* pupfish radiation (33). This recent adaptive radiation (~8000 years old (34)) consisted of at least five species historically(33, 35, 36), including a detritivore (*C. beltrani*), piscivore (*C. maya*), rocky substrate specialist (*C. verecundus*), bivalve specialist (*C. labiosus*), and zooplanktivore (*C. simus*). However, due to recent colonization by native fishes not historically present in the lake and invasive colonization by African tilapia (*Oreochromis niloticus x mossambicus*) (37, 38), all trophic specialist species now appear to be extinct since our collections in 2022, with only the generalist, *C. beltrani*, remaining in 2024 (MK, CM pers. obs.) and 2025 (CG, JSS pers. obs.). Despite exhibiting one of the fastest rates of trait diversification of any vertebrate in tooth size (130 times faster than background rates across *Cyprinodon* (29)) and rapid divergence in other craniofacial morphology (Figure 1A; S1), previous genetic studies of microsatellite data and mtDNA suggest that this radiation has low genetic differentiation (39, 40), enabling the identification of highly differentiated loci among these species.

Results

Genetic differentiation of the species flock

To measure population structure of the Yucatán *Cyprinodon* pupfishes, we collected specimens from the wild in 2022 (Figure 1B) and conducted whole genome resequencing of the

species flock and the coastal sister species (*n* = 15 *C. artifrons*, *n* = 35 *C. beltrani*, *n* = 35 *C. labiosus*, and *n* = 17 *C. simus*). We aligned these samples, as well as eleven other previously sequenced Caribbean pupfish species, to the high-quality *Cyprindon nevadensis mionectes* reference genome (GCA_030533445.1). After calling and filtering variants, our dataset included 23,960,536 SNPs (12.4x mean depth). Using a linkage disequilibrium pruned set of SNPs (*n* = 5,476,855 SNPs), we used principal component analysis and ADMIXTURE to visualize population structure within Yucatán pupfishes. We found that all species formed distinct, non-overlapping genetic clusters, with *C. artifrons* being the most genetically divergent from and sister to the Chichancanab species (Figure 1C). Within the Chichancanab species flock, *C. simus* was more genetically divergent from *C. labiosus* and *C. beltrani* (Figure 1C). These results were also supported by genome-wide F_{ST} estimates and a phylogenetic tree constructed with *ADMIXTOOLS2* (Table S1; Figure S2). Four clusters corresponded to the four different species, as determined by ADMIXTURE (Figure 1D). All *C. artifrons* individuals showed minimal evidence of admixture with Chichancanab species (Figure 1D).

Demographic history

Using MSMC2 for Chichancanab species with a mutation rate of 1.56×10^{-8} substitutions per base pair (estimated from a Caribbean *Cyprinodon* species (26)), we found that the three Chichancanab species (*C. beltrani*, *C. labiosus*, and *C. simus*) diverged from the coastal sister species *C. artifrons* at the end of the Pleistocene 10-15 kya, consistent with receding sea levels resulting in the formation of the Chichancanab lake (34). After divergence from *C. artifrons*, the Chichancanab species flock shows a similar demographic history, characterized by a sharp

decline in effective population sizes, consistent with endemic sympatric species within an isolated lake (Figure 1E).

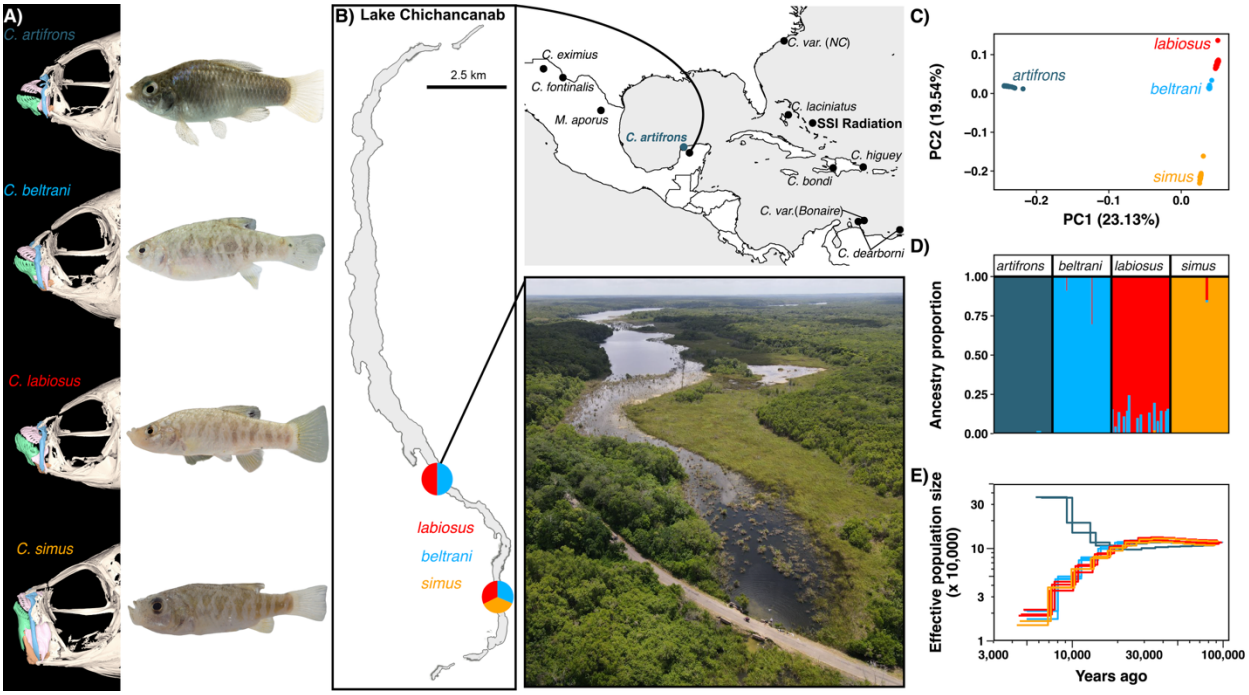

Figure 1. Yucatán *Cyprinodon* pupfishes show strong genetic differentiation. (A) µCT scans of Yucatán pupfish with maxilla colored in blue, premaxilla in pink, dentary in green, and articular in orange (see Figure S1 for different views). (B) Map of the Caribbean showing the sampling sites for all species in our dataset with an inset map of Lake Chichancanab and an aerial view image from one of the sampling sites. (C) Principal component analysis using a set of linkage disequilibrium pruned SNPs. (D) Estimated ancestry proportions for each individual inferred using *ADMIXTURE* with K = 4 (see Figure S3 for K=2-3) from the linkage-pruned dataset. (E) Estimated demographic history with *MSMC2* on a log scale. Each colored line represents an individual, with colors corresponding to different species.

140 *Adaptive loci within trophic specialists*

141 Although genome-wide differentiation among Chichancanab species was moderately low
142 (F_{ST} ranging from 0.032 to 0.09; Figure 2A; Table S1), we were able to identify highly
143 differentiated regions of the genome within the trophic specialist zooplanktivore *C. simus*. We
144 identified 19 fixed and 1,127 nearly-fixed (F_{ST} >0.95) SNPs in *C. simus* relative to other
145 Chichancanab pupfishes (Tables S2-S3). In contrast, we found zero fixed or nearly-fixed SNPs
146 within the generalist *C. beltrani* or bivalve-specialist C. *labiosus*. However, we were able to
147 identify some moderately differentiated SNPs within *C. labiosus* (n = 97) and *C. beltrani* (n =
148 13) relative to the other Chichancanab species at an F_{ST} threshold of 0.8 (Table S2).

149 To search for signals of selection, we calculated the normalized four-taxon population
150 branch statistic (PBS_{nj}; Schmidt et al., 2019) across 10-kb non-overlapping windows because
151 linkage disequilibrium decayed at this distance (Figure S4). Simulation studies demonstrate that
152 normalized *PBS* is effective for identifying both hard and soft selective sweeps (41). Out of the
153 1,146 SNPs fixed or nearly fixed within *C. simus*, 661 were within a strongly supported selective
154 sweep window (top 1% PBS_{nj} outlier (41)), including 425 SNPs within 20 kb of the first or last
155 exon of an annotated gene. These 425 candidate adaptive SNPs ("adaptive variants") were
156 located in the proximity of or within 55 genes (Figure 2A), distributed across 19 out of 24
157 chromosomes (Figure 2A). Adaptive variants associated with the same gene were often
158 distributed across multiple introns or exons and spaced apart by 1kb or more (Figure S5, Table
159 S4).

160

161 *Source and function of adaptive genetic variation in the zooplanktivore*

162 We next characterized the location of the 425 candidate adaptive variants near or within a
163 gene in the zooplanktivore *C. simus*. More than 95% were in intronic or flanking regions (20-kb
164 upstream or downstream of a gene; Figure 2B). Within coding regions, 13 out of 20 adaptive
165 variants were nonsynonymous mutations (Figure 2B). The number of adaptive variants per gene
166 followed an exponential distribution, with a handful of genes containing many variants and most
167 genes with only a single adaptive variant (Figure 2B). We functionally characterized these genes
168 by manually checking online databases and doing a literature search (Table S3; Extended Table
169 S1). 32 out of the 55 candidate genes were associated with craniofacial development (n =11;
170 20%) or sensory/neural function (n = 21; 38.2%). We manually checked if any of these genes
171 overlapped with the 426 unique candidate genes identified in the SSI radiation (26, 28, 30, 32,
172 42–46), and we found only two overlapping candidate genes (*DNM1* and *SPTLC3*), both of
173 which are associated with motor neuron development (47, 48) and are scale-eater-specific
174 candidate genes.
175 Next, we characterized the source of the variants and found that 63% of the adaptive
176 SNPs in *C. simus* also existed as standing genetic variation in the coastal Yucatan population of
177 *C. artifrons* ("standing variation"), 31% were *de novo* variants found only in Chichancanab, and
178 6% were detected as standing genetic variation in other pupfish species but not *C. artifrons*
179 (Figure 2C).

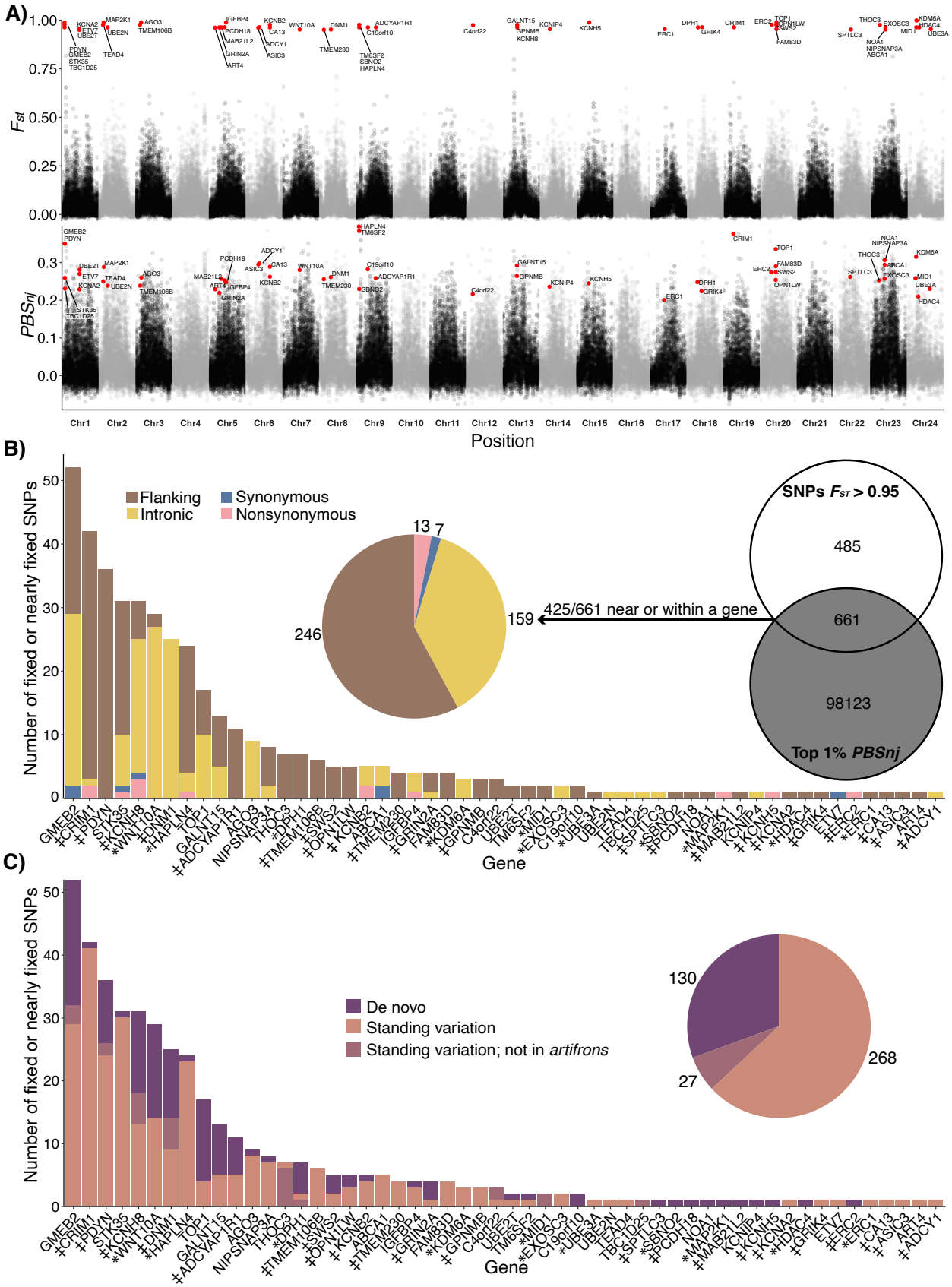
A)
Fst
PBSnj
Position
Chr1
Chr2
Chr3
Chr4
Chr5
Chr6
Chr7
Chr8
Chr9
Chr10
Chr11
Chr12
Chr13
Chr14
Chr15
Chr16
Chr17
Chr18
Chr19
Chr20
Chr21
Chr22
Chr23
Chr24
B)
Number of fixed or nearly fixed SNPs
Flanking
Intronic
Synonymous
Nonsynonymous
13
7
246
159
425/661 near or within a gene
SNPs FST > 0.95
485
661
98123
Top 1% PBSnj
Gene
C)
Number of fixed or nearly fixed SNPs
De novo
Standing variation
Standing variation; not in artifrons
130
27
268
Gene

Figure 2. Architecture and source of adaptive genetic variation in the zooplanktivore. (A, top row) F_{st} between *C. simus* and *C. beltrani* + *C. labiosus* calculated in non-overlapping 10-kb windows. F_{st} values for candidate SNPs (red circles) were calculated separately per locus to show the location of fixed variants. (A, lower row) Population branch statistics (PBS_{nj}) with *C. simus* as the target population versus *C. beltrani*, *C. labiosus*, and *C. artifrons* in 10-kb non-overlapping windows. Candidate genes within 20 kb of fixed or nearly-fixed (Fst > 0.95) SNPs and within PBS_{nj} 1% outlier windows are highlighted in red and labeled. Alternating colors represent different chromosomes. (B) Candidate adaptive variants near or within a gene were defined as SNPs that were fixed (n = 17) or nearly fixed (n = 1,129, F_{st} > 0.95) and occurred within a 1% population branch statistic (PBS_{nj}) outlier window for *C. simus* (Venn diagram). Pie chart and bar graphs indicate the proportion of these 425 adaptive variants that were found within the flanking, intronic, or coding regions. (C) Pie chart and bar graphs indicate the proportion of these 425 variants that were detected only within Chichancanab (de novo: purple), as standing genetic variation in coastal sister species *C. artifrons* (pink), or in other Caribbean species, but not *C. artifrons*. * Indicates genes with a craniofacial annotation; ‡ indicates genes with neural or sensory annotation.

Limited adaptive introgression within Chichancanab pupfishes

To test for introgression into the Chichancanab radiation, we used *f*-statistics calculated in *Dsuite* (49) to examine gene flow from 11 additional *Cyprinodon* species from across the clade and the sister species to the genus *Megupsilon aporus*. Within Yucatán pupfishes, we found evidence of introgression between *C. artifrons* and both *C. beltrani* and *C. labiosus*, with the strongest signal in *C. beltrani* (Figure 3A, B). We also found evidence for introgression between *C. beltrani* and most outgroup species examined, including the sister species to *Cyprinodon*, *Megupsilon aporus*. Relative to *C. beltrani*, *C. labiosus* and *C. simus* also showed evidence of introgression with pupfishes endemic to the Chihuahua desert (*C. eximius* and *C. fontinalis*; Figure 3A, B). Furthermore, we also found evidence of introgression between the two sympatric radiations (*C. variegatus* from SSI) and *C. simus* (Figure 3A, B). However, additional *f*-branch statistics indicate that all patterns of excess allele sharing between these outgroup species besides *C. artifrons* and the Chichancanab species flock likely resulted from ancient introgression events before the colonization of Laguna Chichancanab (Figure 3C; S6).

To test for adaptive introgression into *C. simus*, we next examined whether the set of adaptive variants (Figure 2) occurred within outlier introgression windows using sliding window scans of distance fraction (d_f; Pfeifer & Kapan, 2019) for species that had significant genome-wide introgression into *C. simus* (Figure 3A , B). We found that none of the outlier introgression windows overlapped with *C. simus* adaptive variants (Figure 3D).

Next, we performed *df* scans for introgression between *C. artifrons* and Chichancanab species. Although there were outlier introgression regions between *C. simus* and *C. artifrons* (positive values d_f), these regions did not overlap with *C. simus* adaptive variants (Figure 3D). However, the position of several of these *C. simus* adaptive variants overlapped with outlier

234 introgression windows for both *C. labiosus* and *C. beltrani* but not *C. simus* (Figure 3D). The
235 number of outlier introgression windows was much lower in *C. simus* relative to *C. labiosus* and
236 *C. beltrani* (Figure 3E, F). Furthermore, both *C. labiosus* and *C. beltrani* populations contained
237 several introgression tracts that were much longer than *C. simus* tract lengths, indicating much
238 more recent introgression events in these species (Figure 3E, F).

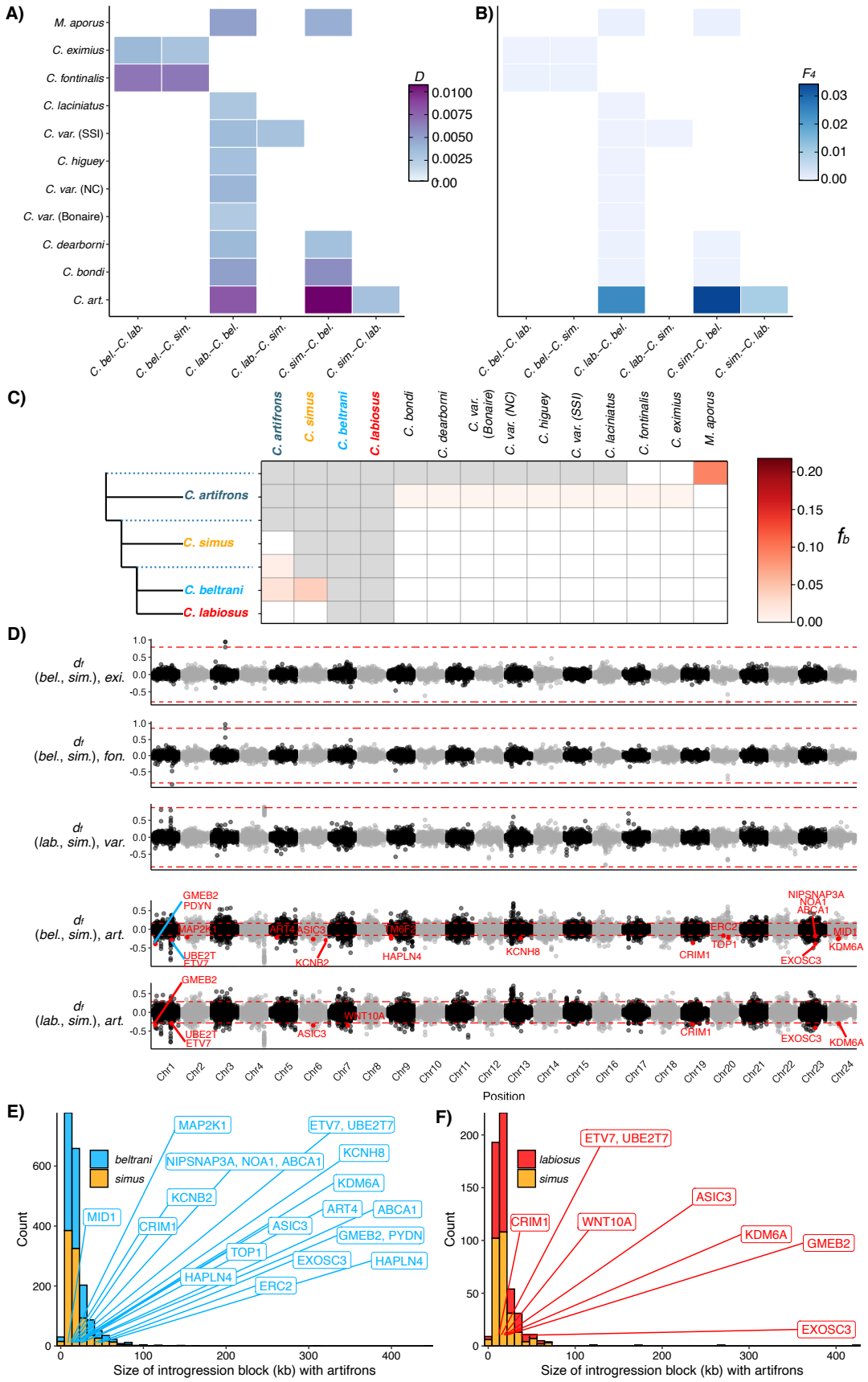
A)
M. aporus
C. eximius
C. fontinalis
C. laciniatus
C. var. (SSI)
C. higuey
C. var. (NC)
C. var. (Bonaire)
C. dearborni
C. bondi
C. art.
C. bel.–C. lab.
C. bel.–C. sim.
C. lab.–C. bel.
C. lab.–C. sim.
C. sim.–C. bel.
C. sim.–C. lab.
D
0.0100
0.0075
0.0050
0.0025
0.00
B)
F4
0.03
0.02
0.01
0.00
C)
C. artifrons
C. simus
C. beltrani
C. labiosus
C. bondi
C. dearborni
C. var. (Bonaire)
C. var. (NC)
C. higuey
C. var. (SSI)
C. laciniatus
C. fontinalis
C. eximius
M. aporus
fb
0.20
0.15
0.10
0.05
0.00
D)
df (bel., sim.), exi.
df (bel., sim.), fon.
df (lab., sim.), var.
df (bel., sim.), art.
df (lab., sim.), art.
GMEB2
PDYN
MAP2K1
UBE2T
ETV7
ART4
ASIC3
KCNB2
TM6F2
HAPLN4
KCNH8
ERC2
TOP1
CRIM1
NIPSNAP3A
NOA1
ABCA1
MID1
KDM6A
EXOSC3
WNT10A
Chr1
Chr2
Chr3
Chr4
Chr5
Chr6
Chr7
Chr8
Chr9
Chr10
Chr11
Chr12
Chr13
Chr14
Chr15
Chr16
Chr17
Chr18
Chr19
Chr20
Chr21
Chr22
Chr23
Chr24
Position
E)
beltrani
simus
Count
MAP2K1
ETV7, UBE2T7
NIPSNAP3A, NOA1, ABCA1
KCNH8
KDM6A
KCNB2
MID1
CRIM1
ART4
ABCA1
ASIC3
GMEB2, PYDN
TOP1
EXOSC3
HAPLN4
HAPLN4
ERC2
Size of introgression block (kb) with artifrons
F)
labiosus
simus
Count
ETV7, UBE2T7
ASIC3
CRIM1
WNT10A
KDM6A
GMEB2
EXOSC3
Size of introgression block (kb) with artifrons

239

Figure 3. Minimal evidence of adaptive introgression into Chichancanab pupfishes. Heatmaps of (A) Patterson's *D*-statistics and (B) F_4 ratios for P1-P2 species combinations within the Chichancanab radiation along the x-axis and P3 focal species along the y-axis. All four-taxon trees used *Cualac tessellatus* as the outgroup (P4). Only significant (*Z*-score > 3) results are colored; combinations not relevant to the Chichancanab radiation are not shown. (C) *f*-branch (f_b) statistics indicate introgression occurring before the Chichancanab radiation. Red boxes indicate significant introgression between P3 species (top row) and the focal species or internal branch (dashed lines) on the left. Non-significant f_b statistics are indicated by white boxes. Grey boxes represent comparisons that cannot be made since f_b cannot be calculated for introgression between sister taxa. See Figure S5 for full *f*-branch graphs. (D) Genome-wide plot of the distance fraction (d_f, an introgression test statistic; Pfeifer & Kapan, 2019) calculated in non-overlapping windows of 91 SNPs (approximately 10 kb) for species trios that showed evidence of introgression with *C. simus*. d_f outlier windows that contained a candidate gene under selection in *C. simus* are colored red and labeled with the gene name. The y-axis label gives the introgression topology: (P1, P2), P3. Positive values indicate regions of introgression between *C. simus* and P3 (from top to bottom: *C. eximius*, *C. fontinalis*, *C. variegatus* (SSI), and *C. artifrons* in the bottom two subplots); negative values indicate regions of introgression between P1 (*C. beltrani* or *C. labiosus*) and P3. Red dashed lines indicate outlier cutoffs, which were determined empirically by the percentage of genome-wide introgression estimated by F_4 ratios in panel B. (E, F) Distribution of the size of d_f outlier introgression tract lengths (in 10 kb windows) between *C. artifrons* and Chichancanab species. The introgression tracts containing candidate adaptive genes in *C. simus* are labeled with gene names. SSI: San Salvador Island, Bahamas; NC: North Carolina, USA.

The stages of adaptive divergence of the zooplanktivore

We used *starTRMCA* (51) to estimate the timing of selective sweeps for the set of candidate adaptive variants near genes within the zooplanktivore *C. simus* (Fig. 4). We estimated that most selective sweeps occurred in a staggered sequence and not simultaneously after colonization of Laguna Chichancanab (Figure 5A)(34). There were also a few older sweeps that we estimate may predate the age of Laguna Chichancanab and divergence from the coastal sister species *C. artifrons* (Figure 1B). Overall, we observed no clear temporal stages of adaptive phenotypic divergence related to craniofacial genes (asterisks: Figure 5) or neural/sensory genes (‡: Figure 5). Instead, we found that selection on these two broad functional categories occurred throughout the period of divergence of *C. simus* following the colonization of Laguna Chichancanab, contrary to expectations of functional stages of adaptation (52) found in the SSI radiation (26).

Next, we used generalized linear regressions to test if sweep age was correlated with the proportion of nonsynonymous adaptive variants, de novo adaptive variants, or the overall number of adaptive variants per gene region. We found that both nonsynonymous adaptive variants ($\chi^2 = 5.852$, $p = 0.016$) and de novo mutations ($\chi^2 = 6.221$, $p = 0.013$) were significantly more likely to occur in more recent selective sweeps during the final stage of adaptive divergence in *C. simus* (Figure 5B, C). However, nonsynonymous mutations were not significantly more likely to be de novo mutations found only in Chichancanab species (All adaptive variants: $\chi^2 = 0.102$, $P = 0.749$; singleton adaptive variants: $\chi^2 = 2.010$, $p = 0.156$), and there was no correlation between estimated sweep age and the number of candidate adaptive variants per gene region ($\chi^2 = 0.111$, $p = 0.740$).

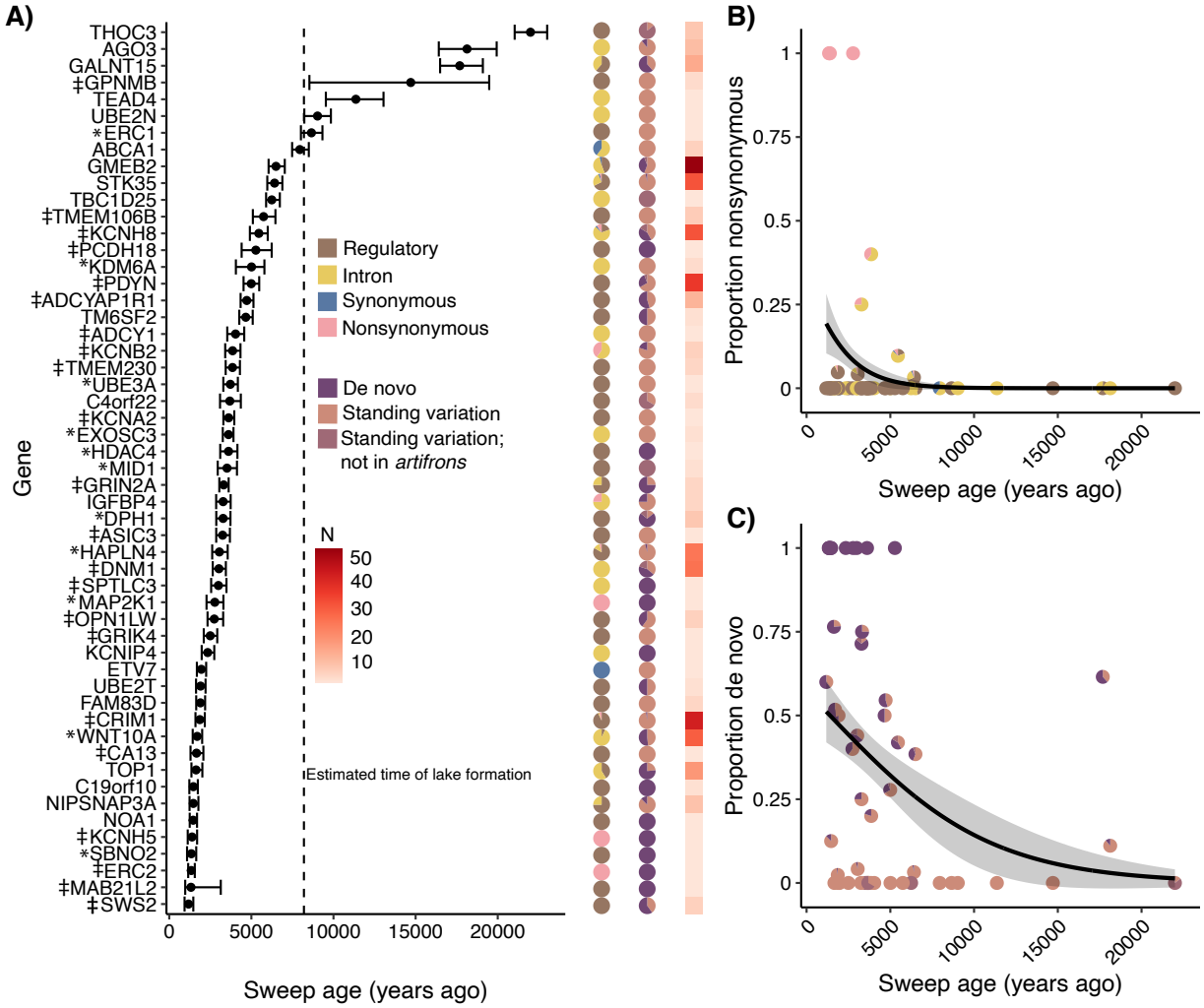

Figure 4. Stages of adaptive divergence in the zooplanktivore. (A) Points indicate median sweep age with 95% credible intervals. The dashed line indicates the approximate age of Laguna Chichancanab (34). For each sweep, the first column of pie charts shows the proportions of flanking/intronic/synonymous/nonsynonymous, second column of pie charts shows the proportions of de novo/standing variation, and third column of squares shows the number of candidate adaptive variants per gene (from Fig. 2). For genes with multiple adaptive variants, we used the variant with the median position as the focal position. * Indicates genes with a craniofacial annotation; ‡ indicates genes with neural or sensory annotation. (B) The proportion of nonsynonymous adaptive variants is significantly larger in more recent selective sweeps, indicated by the best-fit quasibinomial regression line; each pie chart represents a single candidate gene. (C) The proportion of de novo variants is significantly larger in more recent selective sweeps; each pie chart represents a single candidate gene.

Increased visual acuity in the zooplanktivore is consistent with vision-related candidate adaptive genes

We identified several *C. simus* adaptive variants associated with eye development (*ASIC3*(53), *CRIM1*(54), *MAB21L2*(55)) and opsin (*OPN1LW*, *SWS2*) genes (Table S1). Because the trophic specialization of *C. simus* requires visually locating zooplankton in the open water before targeted suction-feeding strikes, we hypothesized that this species would have higher visual acuity than the detritivore, *C. beltrani*. We conducted optomotor response trials on lab-reared individuals from both species (F1 *C. beltrani* and long-term laboratory colony of *C. simus* (F10+)) and found that *C. simus* has a much stronger optomotor response than *C. beltrani* in response to black-and-white vertical bars spinning at a constant rate of approximately 90 rotations per minute (Figure 5A, B; Wilcoxon signed-rank test: $W = 1$, $P = 0.009$). There was no significant difference in rotations per minute between the species for the same individuals during control observation periods with no spinning (Figure S7A; $W = 14$, $P = 0.3105$) or during positive control observation periods with an all-black background spinning at the same frequency (Figure S7B; $W = 9$, $P = 0.147$).

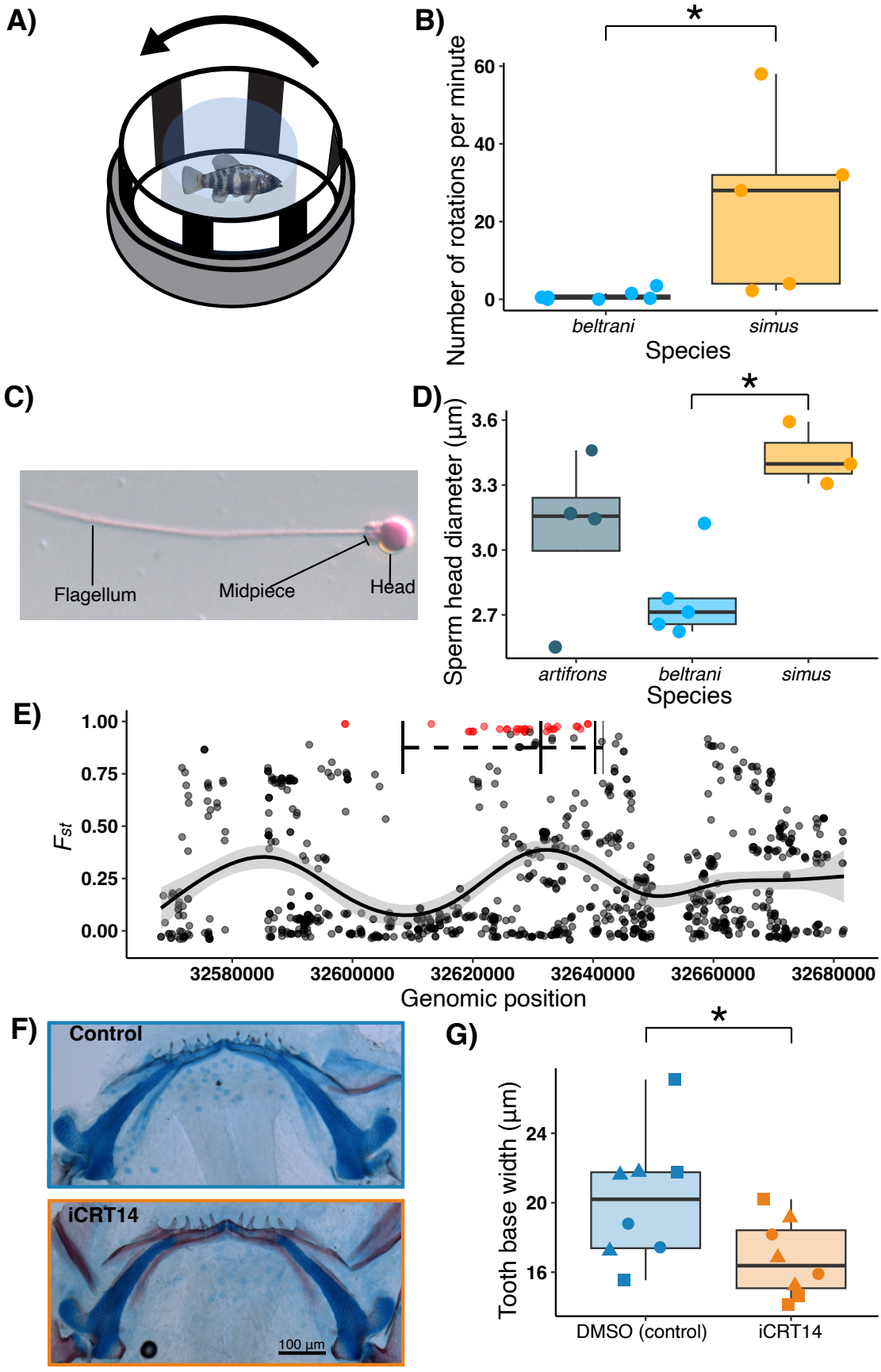
A)
B)
*
Number of rotations per minute
60
40
20
0
beltrani
simus
Species
C)
Flagellum
Midpiece
Head
D)
*
Sperm head diameter (µm)
3.6
3.3
3.0
2.7
artifrons
beltrani
simus
Species
E)
1.00
0.75
0.50
0.25
0.00
Fst
32580000
32600000
32620000
32640000
32660000
32680000
Genomic position
F)
Control
iCRT14
100 µm
G)
*
Tooth base width (µm)
24
20
16
DMSO (control)
iCRT14

326

Figure 5. Divergence in visual acuity, sperm morphology, and tooth development reflect candidate adaptive genes in the zooplanktivore. (A) Diagram of the optomotor response experimental apparatus (adapted from Neuhauss et al., 1999). (B) Boxplot and jittered points of the number of complete rotations fish swam per minute, indicative of their optomotor response to black-and-white vertical bars spinning at a constant rate. (C) Representative labeled image of a single *C. beltrani* sperm at 100x stained with rose bengal. (D) Boxplots with jittered points of sperm head diameter for *C. artifrons, beltrani,* and *simus.* Significant Tukey's post hoc differences are shown with an asterisk. (E) Manhattan plot showing per-site F_{st} of SNPs within 50 kb of WNT10A. Black rectangles indicate exons of WNT10A, and dashed lines indicate introns. Red points represent nearly fixed SNPs ($F_{st} > 0.95$), and black points represent all other SNPs. The black line is the smoothed average F_{st} in this region, with grey shading being the 95% confidence intervals. (F) Representative image of *C. beltrani* larvae that were treated with DMSO (control; top) or with iCRT14 Wnt inhibitor + DMSO (bottom) and stained with alizarin red (bone) and alcian blue (cartilage). (G) Boxplot and jittered points of average tooth base width of the left and right teeth closest to the mandibular symphysis for *C. beltrani* larvae treated with either a control or Wnt inhibitor (iCRT14). Shapes represent different split-brood replicates.

Divergent sperm morphology of the zooplanktivore is consistent with spermatogenesis-related candidate adaptive genes

Four candidate genes (*C4orf22*, *STK35*, *ERC2*, and *TBC1D25*) are known to affect spermatogenesis/fertility (57–60). We therefore examined whether three Yucatan species, raised in a common garden laboratory environment (F1 *C. artifrons,* F1 *beltrani,* and a long-term laboratory colony of C. *simus* F10+), differed in sperm morphology using differential interference contrast microscopy. We found that species significantly differed in sperm head length (Figure 5D; $F = 5.724$, $p = 0.025$), but not sperm midpiece length (Figure S7A; $F = 2.403$, $p = 0.147$) or flagellum length (Figure S8B; $F = 0.414$, $p = 0.673$). Tukey's post hoc pairwise comparisons indicated that *C. simus* had significantly larger sperm heads than *C. beltrani* ($q = 3.367$; $p = 0.0207$; Fig. 5D).

Inhibition of WNT10A alters tooth morphology in Chichancanab pupfish

We identified a large number of highly differentiated SNPs surrounding the well-characterized *WNT10A*, which controls tooth, hair, and skin development within the Wnt signaling pathway (Figure 2; Figure 5E (61–63)). This is consistent with the most exceptional morphological difference between *C. simus* and *C. beltrani,* extreme divergence in tooth size (100 times faster than background rates (29)).

To test for the importance of *WNT10A* in tooth development within pupfishes, we used iCRT14 to inhibit the Wnt / β catenin pathway downstream of WNT10A during metamorphosis in *C. beltrani* lab-reared fry (64, 65). Chemical inhibition from 8 dpf to 23 dpf resulted in narrower teeth than control fry treated with DMSO ($\chi^2 = 4.840$, $P = 0.0278$; Figure 5F, G). There were no significant differences in mean tooth length ($\chi^2 = 0.455$, $p = 0.500$; Figure S9) or number of ossified teeth when stained with alizarin red ($\chi^2 = 0.114$, $p = 0.7357$; Figure S10).

Discussion

Here, we investigated the genetic architecture, sources of adaptive variation, and temporal dynamics of selection underlying speciation and trophic specialization in a young adaptive radiation of *Cyprinodon* pupfishes endemic to Laguna Chichancanab, Mexico. By comparing these patterns to our previous work on a recent radiation of *Cyprinodon* pupfishes in SSI, Bahamas (26, 28–32), we discovered parallel and non-parallel features of these independent radiations in similar environments. Despite replicate radiations of Caribbean pupfishes in large, isolated, predator-free, saline lakes with few competitors, we found little parallelism between the radiations. Although craniofacial morphology diverged rapidly within trophic specialists in both radiations, we found almost zero overlap in the adaptive genes underlying trophic specialization,

potentially reflecting the divergent specialists within each radiation. In contrast to SSI, there was no behavior-first stage of adaptive divergence in Chichancanab specialists and, with the exception of craniofacial development, candidate adaptive gene ontologies potentially relevant to speciation were not shared, such as pigmentation genes in SSI versus opsin and spermatogenesis genes in Chichancanab. Unlike the SSI radiation and most other well-studied adaptive radiations (e.g., Malawi cichlids (20), Galápagos finches (66)), adaptive introgression likely played a minimal role in the Chichancanab radiation. We found no overlap between adaptive variants in the specialists and tracts of introgression. Instead, over 30% of the candidate adaptive variants in the zooplanktivore, *C. simus*, likely arose from de novo mutations compared to only 2% in the SSI scale-eater specialist and 0% in the molluscivore specialist. One outstanding parallel feature was a clear stage of refinement in the adaptive divergence of the zooplanktivore, marked by increased rates of de novo and nonsynonymous adaptive mutations occurring among the most recent selective sweeps in this species, similar to the scale-eating specialist on SSI.

Adaptive introgression did not contribute to speciation of Chichancanab pupfishes

Genomic analyses have revealed that hybridization and adaptive introgression played a major role in many adaptive radiations (3, 3, 16, 19–27, 67, 68), including the *Cyprinodon* SSI radiation (26, 31). However, in Chichancanab, we found minimal evidence of introgression overall and did not detect any signatures of adaptive introgression following the colonization of Laguna Chichancanab. Although our analyses indicate extensive introgression among Cyprinodontidae lineages, we did not find any introgression events into the root of the radiation, nor has there been secondary gene flow from outgroup species other than the sister species to the radiation, *C. artifrons*. Secondary gene flow from *C. artifrons* was almost entirely detected with

404 *C. beltrani* and, to a lesser extent, *C. labiosus.* Gene flow may be higher with these species
405 because *C. artifrons,* a coastal benthic feeding detritivore, is less ecologically divergent from
406 both *C. beltrani,* a benthic feeding detritivore, and *C. labiosus*, a benthic feeding bivalve
407 specialist. Secondary gene flow between *C. artifrons* and *C. beltrani* and *C. labiosus* overlapped
408 with many genes under selection in *C. simus*, suggesting that secondary gene flow is potentially
409 helping to increase similarities between the benthic detritivores within the lake and the coast
410 rather than by bringing in new adaptive variation for trophic specialization in *C. simus*.
411 These results are remarkably different from the *Cyprinodon* adaptive radiation of SSI,
412 where there is strong evidence of introgression into the root of the radiation and substantial
413 evidence of secondary adaptive introgression into both trophic specialists from at least three
414 different biogeographic regions of the Caribbean and Atlantic coast (26, 31). Laguna
415 Chichancanab is an endorheic basin with no above-ground hydrological connections to the ocean
416 and is substantially more geographically isolated than SSI, a small island in the approximate
417 center of the Caribbean. Furthermore, the sister species to the Chichancanab species flock, *C.*
418 *artifrons*, is abundant along the entire coast of the Yucatán peninsula, suggesting that any gene
419 flow into Chichancanab would likely first have to pass through *C. artifrons* populations. An
420 additional factor is the water chemistry of Laguna Chichancanab which is near-saturation with
421 calcite and gypsum and may be a greater physiological barrier to marine pupfish colonists than
422 the slightly hypersaline lakes of SSI. Thus, geography and ecology play an important role in
423 determining the relative importance of adaptive introgression in radiations.
424
425 *De novo mutations primarily drive adaptive divergence of the zooplanktivore*

426 The importance of de novo mutations in adaptive radiations remains contentious, in part
427 due to the time needed for de novo beneficial mutations to arise (11, 15). Interestingly, we find
428 that 30.6% of the zooplanktivore adaptive variants were detected only within Chichancanab
429 species, suggesting their de novo origins within the basin. This proportion is 15.3 times greater
430 than the contribution of de novo mutations to adaptive divergence of the scale-eater in the SSI
431 radiation. A primary factor could be that the estimated effective population size for the
432 Chichancanab radiation is approximately twice that of the SSI radiation (26), indicating that
433 selection on de novo mutations is more effective, with a higher probability of fixation, all else
434 being equal (14). There may also be a lack of existing standing genetic variation within
435 Caribbean pupfish populations that is adaptive for zooplanktivory. In support of this hypothesis,
436 although radiations should proceed along genetic lines of least resistance (69), the primary axis
437 of craniofacial morphological variation along which the zooplanktivore has diverged is
438 orthogonal to the major axes of variation that within Caribbean pupfish species (29). Evolving
439 along the line of greatest resistance instead of least resistance may require de novo mutations.
440 While the SSI scale-eater is also highly divergent, it is closer to the existing morphological space
441 of Caribbean pupfish species and in the direction of greatest variance along the first two
442 principal component axes (29). Similarly, mutational target size for the craniofacial features of a
443 zooplanktivore may be much smaller than the features of a scale-eater, resulting in less standing
444 genetic variation available for adaptation to this trophic niche. Alternatively, we may not have
445 detected these de novo mutations in other populations, but this is unlikely to explain all de novo
446 mutations given our extensive sampling of *Cyprinodon* species across the clade and spanning the
447 Caribbean (Fig. 1). Thus, our results highlight that de novo mutations may play a more important

role in driving young adaptive radiations than currently appreciated (12, 13), especially when ecotypes are highly divergent from other species within the radiation.

Minimal parallelism in the genes underlying adaptive divergence of trophic specialists

We found only two candidate genes (*DNM1* and *SPTLC3*) among the 55 zooplanktivore candidate genes in the Chichancanab radiation that overlapped with the hundreds of candidate genes identified so far in the SSI radiation (26, 28, 30, 32, 42–46). Consistent with trophic specialization requiring the pursuit of mobile prey, both genes are involved in motor neuron development. *DNM1* is a dynamin with nervous tissue-specific expression that is crucial for the proper formation of motor neuron axons (47). *SPTLC3* is involved in the biosynthesis of sphingolipids (70), and suppression of *SPTLC3* in zebrafish results in motor neuron axon defects (48).

The extremely limited number of shared adaptive genes is surprising given the high conservation of gene function in both morphological development (71, 72) and behavior (73), and the frequent parallelism of candidate genes across vertebrate adaptive radiations, particularly for craniofacial genes. For example, *BMP4* is involved in diversification in both Galápagos finches (74) and African cichlids (75, 76). Furthermore, within the SSI radiation, many of the same genes show parallel patterns of differential expression even within divergent trophic specialists (26, 43). Nonetheless, parallelism of shared regulatory networks, rather than specific genes, is still a possibility.

Rapid divergence in tooth morphology of the zooplanktivore through WNT10a

470 Another reason for this non-parallelism is that trophic specialists in each radiation have
471 diverged in different sets of traits during adaptation to different ecological niches (29).
472 Specifically, the Chichancanab radiation has diversified in tooth size over 130 times faster than
473 background rates, driven by the extremely short and narrow teeth of the zooplanktivore (Figure
474 S1; (29). We identified a well-characterized tooth development gene in the Wnt pathway,
475 *WNT10A*, with many de novo mutations in flanking (n = 2) and intronic (n = 13) regions.
476 Mutations in *WNT10A* are associated with tooth developmental disorders in humans (62) and
477 both knockout and overexpression experiments in sticklebacks and zebrafish have demonstrated
478 *WNT10A*'s role in teeth development and regeneration (61, 63). Consistent with *WNT10A*
479 playing a role in rapid divergence of tooth morphology, we found that inhibiting the Wnt
480 pathway in the *C. beltrani* generalist during pre-metamorphosis development resulted in
481 narrower teeth, similar to the reduced tooth sizes in the zooplanktivore *C. simus* (Fig. 4c). This
482 indicates that the substantial number of de novo mutations in WNT10a may be suppressing the
483 Wnt pathway, resulting in a large phenotypic effect on tooth size reduction in the zooplanktivore.
484

485 *Increased visual acuity in the zooplantkivore is consistent with unique selection on vision-related*
486 *genes*

487 One of the more striking features of both *Cyprinodon* radiations is the evolution of novel
488 trophic specialists from a generalist ancestor: the scale-eater (*C. desquamator*) in the SSI
489 radiation and the zooplanktivore (*C. simus*) in the Chichancanab radiation. Although these are
490 distinct dietary specializations, they share a similarity in that they require tracking free-
491 swimming prey. Indeed, four of the top 15 enriched GO terms of candidate genes in the SSI
492 scale-eater were related to eye development (26). Similarly, several of the candidate genes we

493 identified in the zooplanktivore were related to eye development, including *ASIC3*, *MAB21L2*,
494 and *CRIM1*. *CRIM1* is the most promising candidate because it is one of the few candidate genes
495 with multiple nonsynonymous mutations (Figure 2B). In zebrafish, a two-base pair deletion in
496 *CRIM1* resulted in abnormal lenses as well as a large eye-to-head ratio (54). Interestingly, one of
497 the defining morphological features of *C. simus* is its large eye-to-head ratio (33) (Figure 1A).
498 Consistent with candidate genes related to eye development, we confirmed that *C. simus* exhibits
499 a much stronger optomotor response than *C. beltrani*, indicating that this specialist has greatly
500 improved visual acuity, even when reared in a common laboratory environment.
501 Although both radiations contained many vision-related candidate genes, selection on
502 opsin genes was unique to Chichancanab. Most notably, we found several adaptive variants
503 associated with *SWS2* (blue-sensitive), and *OPN1LW* (red-sensitive) in the zooplanktivore.
504 Interestingly, both opsins contain many candidate de novo mutations, and *SWS2* is the youngest
505 selective sweep in the zooplanktivore. One explanation could be that most Caribbean
506 *Cyprinodon* species are benthic and live in similar habitats, resulting in limited standing genetic
507 variation in opsins. Additionally, most environments (including SSI and Chichancanab) are
508 relatively shallow, so differences in depth—a common selective pressure on opsin evolution
509 (77)—are likely not a strong selective force on SSI. Thus, the main selective force acting on
510 vision in Chichancanab may be prey capture efficiency. In many fish species, zooplanktivory is
511 associated with higher expression of shorter wavelength opsins (e.g., *SWS1* (77)), whereas
512 piscivory is not often associated with changes in opsin expression (78, 79).
513
514 *Divergent sperm morphology in Chichancanab species consistent with selection on*
515 *spermatogenesis genesis*

516 Although the role that premating sexual selection plays in speciation has historically been
517 the main focus (80, 81), there is both theoretical and empirical support for the role of postmating
518 sexual selection in maintaining reproductive isolation via postmating prezygotic reproductive
519 barriers (82–87). In the SSI radiation, species differ in pigmentation, and a handful of the
520 candidate adaptive variants fall in regulatory regions of genes associated with pigmentation (26),
521 but not spermatogenesis. Furthermore, there is evidence for premating isolation by female
522 preference in the scale-eater (88). However, in Chichancanab, the two species tested in our data
523 set (*C. labiosus* and *C. beltrani*) were not found to visually distinguish between different species
524 in the radiation (89).
525 Unlike the SSI radiation, we did not find any candidate adaptive variants associated with
526 pigmentation in Chichanancab; instead, we identified adaptive variants associated with four
527 spermatogenesis genes, *ERC2*, *TBC1D25*, *C4orf22*, and *STK35*. Consistent with previous work
528 demonstrating the importance of these genes in spermatogenesis (57–60), we found that *C. simus*
529 does indeed have larger sperm heads than *C. beltrani*, suggesting a unique role for post-mating
530 prezygotic reproductive barriers in this radiation (Fig. 4b).
531
532 *Parallelism in the stages of adaptation: refinement with de novo and nonsynonymous mutations*
533 Adaptation may occur in stages, with less pleiotropic cis-regulatory changes occurring
534 before potentially more pleiotropic amino acid changes (26, 90, 91). Selection is also predicted
535 to act on standing variation first (14, 92). In both radiations, we observed strong evidence for a
536 refinement stage of coding substitutions occurred last. In Chichancanab, these late-sweeping
537 coding substitutions were also de novo mutations (Fig. 3). The simplest explanation for
538 parallelism in more recent ages of adaptive de novo mutations is the waiting time required for

539 beneficial mutations to (1) arise and (2) reach a substantial frequency within the population (14,
540 92). These variants may only be selected in the later stages of an adaptive walk because
541 nonsynonymous mutations are often pleiotropic and likely deleterious in the ancestral genetic
542 background (14, 93). Thus, they may not be advantageous until later in the adaptive walk, where
543 sign epistasis may reverse negative pleiotropic effects (94–98). Our results highlight that this
544 final refinement stage is likely a general pattern during adaptive divergence.
545

546 **Methods**

547 *Sampling*

548 We collected Laguna Chichancanab specimens in 2022 over two days using a 5 x 1.3 m
549 seine net with 1.6 mm mesh size. We sampled two sites, an entrance road by La Presumida, and a
550 bridge crossing the narrow section of the lake on the road to San Diego. *C. labiosus* and *C.*
551 *beltrani* were sampled from both sites for this study, whereas *C. simus* was only collected at La
552 Presumida. *C. artifrons* were collected by cast net from the coastal estuary at Sisal. Additional
553 specimens were collected from the Bahamas (Lake Cunningham, New Providence Island and
554 Crescent Pond, San Salvador Island), the Dominican Republic (Laguna Bavaro), or Fort Fisher,
555 North Carolina as described previously (Martin 2016) or sourced from the American Killifish
556 Association, the London Zoological Society, the Dallas Children's Aquarium, and Frans
557 Vermuelen. All specimens were euthanized in an overdose of buffered MS-222 (Fiquel, Inc.)
558 following approved animal care and use protocols from the University of California, Berkeley
559 and the University of California, Davis.
560

561 *Sequencing, Variant calling and filtering*

562 Individual DNA samples were resequenced using Illumina Hiseq 4000 and Novaseq. Raw
563 reads were trimmed with *fastp* (v0.23.4) (99). Reads were mapped to the UCB_CyNevMio_1.0
564 *Cyprindon nevadensis mionectes* reference genome (GCA_030533445.1) with *bwa mem*
565 (v0.7.17) (100). Duplicate reads in the bam files were marked with *Picard MarkDuplicates*
566 (GATK v4.5.0.0) (118). Coverage and mapping quality were assessed with *qualimap* (v2.2.2)
567 (101). We followed the *GATK* (v.4.5.0.0) genotyping pipeline to call variants (119). We used
568 *HaplotypeCaller* (-ERC GVCF) v4.5.0.0 to call variants for each individual and stored variants
569 in the GenomicsDB datastore format prior to using *GenotypeGVCFs* to perform joint
570 genotyping. We restricted our analyses to biallelic SNPs and applied the recommended *GATK*
571 hard filters (QD < 2, QUAL < 30, SOR > 3, FS > 60, MQ < 40, MQRankSum < -12.5,
572 ReadPosRankSum < -8) to filter SNPs (118, 120). Missing genotypes were reset to ./. from 0/0
573 due to how *GATK* represents missing genotypes in version 4.5.0.0 (105).
574 After hard-filtering and variant calling, we filtered the data set further by removing SNPs
575 with minor allele frequency < 0.05, more than 10% missing, depth less than 10x, and GQ less
576 than 20 using *BCFtools* (v1.16)(106). This resulted in a final data set that included 23,960,536
577 SNPs.
578
579 *Population structure of Yucatán Cyprinodon pupfishes*
580 To assess population structure, we first pruned SNPs in linkage disequilibrium using
581 *PLINK* (v. 1.9) with the following parameters: "-indep-pairwise 50 5 0.2" (107). This filtered our
582 data set from 23,960,536 SNPs to 5,476,855 SNPs. With this linkage disequilibrium pruned data
583 set, we first filtered the full VCF file to only include relevant Yucatán *Cyprinodon* species (i.e.,
584 *C. artifrons, C. beltrani, C. labiosus,* and *C. simus*), then conducted a PCA using *PLINK*. Next,

585 we used *ADMIXTURE* (v1.3) to determine the optimal number of population clusters that best fit
586 the data and to assign individuals to their corresponding population clusters (108). We performed
587 this analysis and calculated cross-validation error for the number of clusters K = 1-6. Models in
588 ADMIXTURE with K=2-4 were equally supported (Figure S2A). However, given morphological
589 distinctness and the results of the PCA, we present the results for when K = 4 (Figure 1D).
590
591 *Demographic history of Yucatán Cyprinodon pupfish*
592 We estimated demographic history using *MSMC2* (109). For each Yucatán pupfish
593 species, we selected three individuals with the highest mean depth and generated single-sample
594 VCF files, individual mask files, and "mapability" mask files. We then ran *MSMC2* with default
595 parameters except we set phasing to "unphased" and "P_PAR=8*1+25*1+1*2+1*3." For
596 plotting, we used a generation time of 1 year and a mutation rate of 1.56×10^{-8} substitutions per
597 base pair, estimated from Caribbean *Cyprinodon* species (26).
598
599 *Identifying candidate genes*
600 We calculated F_{st} genome-wide, per site, and in non-overlapping 10-kb windows using
601 the "--weir-fist-pop" function in *VCFtools*(v0.1.16) for all pairwise combinations of Yucatán
602 *Cyprinodon* species (110). We chose 10-kb windows because linkage disequilibrium was
603 substantially decayed at this distance (Figure S3), and these windows allowed us to quantify
604 finer-scale genomic variation. With the 10-kb windowed F_{st} values, we calculated a modified
605 population branch statistic (PBS) for four taxa, PBS_{nj} (111). This statistic is useful because it
606 makes no assumptions about species topology or polarization (111). We then normalized PBS_{nj}
607 by the total tree length, as normalized *PBS* is most effective and specific at identifying selective

608 sweeps (41). We classified SNPs as candidates if they were fixed or nearly fixed (per-site F_{st}
609 >0.95) compared to other species within the radiation and were among the top 1% outliers out of
610 all PBS_{nj} windows, following the threshold used in (41).
611
612 *Introgression*
613 Using the full VCF file, which contained a wide range of species in the family
614 Cyprinodontidae, we tested for evidence of introgression in Yucatán *Cyprinodon* species using
615 *Dsuite* (49). We first excluded any samples/species that had an average depth < 4. We then
616 calculated all possible trios with a species tree based on the most recent phylogeny (112) with
617 *Cualac tessellatus* as the outgroup. We calculated Z-scores to assess the significance of *D*
618 statistics using 1,000 jackknife blocks and considered a Z-score greater than three as evidence
619 for significant introgression (113). We only focused our primary analysis on species trios where
620 P1-P2 included species within the Laguna Chichancanab radiation. We used the other trio
621 calculations to calculate *f*-branch (f_b) statistics to account for correlated f_4-ratio scores and to
622 inform the timing of introgression events (49).
623 For species trios that showed evidence of introgression where *C. simus* was either P1or
624 P2, we then calculated the distance fraction (d_f), a robust metric of introgression for windowed
625 analyses (50), in non-overlapping windows of 91 informative SNPs. We chose this number of
626 SNPs because it resulted in windows of approximately 10 kb. We considered windows to be
627 introgressed if they were in the top X% of absolute d_f value, where X% was the percentage of
628 estimated genome wide introgression (e.g, f_4-ratio) (114, 115). To estimate introgression block
629 sizes, we merged neighboring windows that were both introgression outliers and took the total
630 size of the blocks.

631

632 *Characterizing candidate genes*

633 After identifying candidate SNPs, we then used *Bedtools* (v2.31) to see if SNPs occurred
634 near (20-kb) or within a gene (116) with a GFF annotation file for the *C. nev. mionectes*
635 reference genome (Tian et al. in prep). We classified SNPs within 20 kb of a gene (upstream or
636 downstream) as flanking. For SNPs within a gene, we further classified them into intronic,
637 synonymous, or nonsynonymous using *SnpEff* (117).

638 To characterize the origin of candidate SNPs, we extracted the alleles from every species
639 for each candidate SNP. We classified variants that were found in any other species as "standing
640 variation". We further subdivided this group into variants that were found in other species but not
641 in *C. artifrons*. If "standing variation" variants fell within an introgression window, we classified
642 them as "introgressed." Finally, if the alternative variant was only found in Chichancanab
643 species, we classified it as de novo.

644

645 *Timing of selective sweeps*

646 To gain insight into the timing of selective sweeps in *C. simus*, we used *starTRMCA* (51).
647 Because many genes contained multiple candidate SNPs, for this analysis, we selected the
648 variant that was in the median position of each gene. We then extracted a 1-Mb region
649 surrounding that variant and removed all sites that contained missing data. For simplification, we
650 only used the generalist/detritivore, *C. beltrani*, as the "reference" population and the
651 zooplanktivore, *C. simus*, as the "selected" population. We used a fixed recombination rate of
652 $2x10^{-8}$ (swordtail fishes; (118)) and a mutation rate of $1.56x10^{-8}$ substitutions per base pair
653 (Caribbean *Cyprinodon* species; 26). We then ran five separate Markov chains for 30,000

654 iterations with a proposal standard deviation of 150 (preliminary analyses changing this
655 parameter had minimal influence on results). We then discarded the first 10,000 iterations of each
656 chain as burn-in.

657 To test for stages of adaptation, we conducted separate generalized linear regressions to
658 test if the sweep age was correlated with the proportion of nonsynonymous SNPs, proportion of
659 de novo SNPs, and the number of SNPs. For the generalized linear regressions of proportion of
660 nonsynonymous SNPs and proportion of de novo SNPs, we used a quasi-binomial family to
661 account for overdispersion with a logit link function. For the number of SNPs, we used a quasi-
662 Poisson family with a log link function. To test for the significance of sweep age, we used a
663 likelihood ratio test comparing a model with the estimated sweep age as an effect compared to a
664 null model.

665

666 *Optomotor response*

667 We tested for differences in visual acuity between the generalist/detritivore, *C. beltrani*,
668 and the zooplanktivore, *C. simus*, by conducting an optomotor response behavioral assay. We
669 tested lab-reared *C. beltrani* (F1, $n = 7$) and lab-reared *C. simus* (long-term laboratory colony
670 exceeding ten generations in the lab, $n = 5$). Each fish was tested consecutively with each control
671 or treatment for 1-minute observation periods, with the control observation occurring first,
672 followed by presentation of all-black and black-and-white spinning bars. The order of
673 presentation for the latter to treatments was alternated in each trial. Fish were placed in a
674 suspended cylindrical plastic container 0.3 m in diameter that remained stationary during the
675 course of the trials. Spinning black-and-white or all-black paper was rotated outside the clear
676 plastic container at an RPM of ~90rpm during each observation period.

Due to the data being nonparametric (count, zero-inflated, unequal variance between groups), we conducted a Wilcoxon rank sum test for the on-banded (all black) and on-banded portions separately. Because we had an a priori hypothesis that *C. simus* would display a stronger optomotor response (greater visual acuity), we calculated *p*-values with a one-tailed test.

Sperm morphology

To test for differences in sperm morphology, we collected sperm samples from five individuals per species in the lab (*C. simus, C. artifrons, C. beltrani*). We first anesthetized the fish with a solution of MS-222. After the fish was anesthetized, we collected 1μL of milt (fish semen) with a 1μL glass microcapillary tube and fixed the sample overnight in a 4% PFA solution stained with Rose Bengal. We then plated sperm on a positively charged slide with a sealed coverslip. We imaged sperm with oil immersion with a 63x objective and measured 10-30 sperm per individual in ImageJ (119). Due to poor sperm samples from some individuals (little sperm), we ended up with the following sample sizes: three *simus*, four *artifrons*, and five *beltrani*.

To retain information about variation within individuals, we fit separate linear mixed-effects models for each trait of interest (sperm head, midpiece, and flagellum lengths) with population as a fixed effect and a random intercept for individual ID, using *LME4* (120). To assess the significance of the model, we used a Type II ANOVA with a Wald *F* test using Kenward-Roger degrees of freedom. If there was a significant effect of population, we conducted post hoc pairwise tests using the *Emmeans* package (121) and corrected for multiple comparisons using the Tukey method. We did not correct for phylogeny due to how closely related the species

699 are, the limited sample size, and the fact that the only significant differences were between sister
700 species.
701
702 *Wnt inhibition experiment*
703 To confirm the role of the Wnt pathway in proper jaw and teeth development, we
704 conducted an experiment chemically inhibiting the Wnt pathway using iCRT14 during
705 metamorphosis in *C. beltrani*. To control the exact time of development, we first performed in
706 vitro fertilizations and incubated developing embryos at 24 °C until hatching (~8dpf). On the day
707 of hatching, we haphazardly split broods into control and experimental groups to control for
708 batch and family effects. We raised experimental groups in tank water with a 100 nanomolar
709 concentration of iCRT14 and control groups in a 100 nanomolar concentration of DMSO
710 (solution used to dilute stock iCRT14). We ran the experiment for two weeks until individuals
711 were (22dpf), changing the solution every 3-4 days. We performed this experiment on four
712 separate broods (~12 individuals/treatment). One brood was excluded as there was improper
713 development (no ossification of the spine) in the controls.
714 After the experiment, we euthanized fish with MS-222 and stained fish with alizarin red
715 (bone) and alcian blue (cartilage) following a modified published protocol (122). After staining,
716 we prepared whole mounts and imaged fish with fluorescent microscopy (Zeiss LSM880 FCS)
717 to quantify ossification of the jaw and teeth (123). We then dissected out the lower jaw and
718 prepared flat mounts to measure teeth morphology. Specifically, we measured the tooth length
719 and base width for the left and right teeth closest to the mandibular symphysis. For statistical
720 analyses, we averaged these values.

We fit separate linear mixed-effects models for tooth length and base width with experimental treatment as a fixed effect and a random intercept for brood/replicate, using *LME4* (120). For the number of ossified teeth, we used a generalized linear mixed-effect model with a Poisson family and log-link function. To assess the significance of these models, we used a likelihood ratio test comparing it to a null model without treatment as a fixed effect.

Acknowledgments

MCK was supported by a Miller Postdoctoral Research Fellowship from the Miller Institute for Basic Research in Science, University of California Berkeley. This research was funded by NSF CAREER 1749764, NIH 5R01DE027052-02, Daphne and Ted Pengelley Award from the Center for Population Biology, and ARCS Foundation awards to CHM. We thank the Gerace Research Center and Troy Day for logistical support in the Bahamas, and the governments of Mexico and the Bahamas BEST commission for permission to collect and export samples (Permit No. PPF/DGOPA-001/20). All research procedures and animal care protocols (AUP-2021-02-14062-1 and AUP-2021-07-14515) were approved by the University of California, Berkeley Animal Care and Use committee and the UC Davis Institutional Animal Care and Use committee.

References

1. R. G. Gillespie, *et al.*, Comparing Adaptive Radiations Across Space, Time, and Taxa. *J Hered* **111**, 1–20 (2020).

2. C. H. Martin, E. J. Richards, The Paradox Behind the Pattern of Rapid Adaptive Radiation: How Can the Speciation Process Sustain Itself Through an Early Burst? *Annual Review of Ecology, Evolution, and Systematics* **50**, 569–593 (2019).

745 3. Y. Naciri, H. P. Linder, The genetics of evolutionary radiations. *Biological Reviews* **95**,
746 1055–1072 (2020).

747 4. D. Schluter, *The Ecology of Adaptive Radiation* (OUP Oxford, 2000).

748 5. J. T. Stroud, J. B. Losos, Ecological Opportunity and Adaptive Radiation. *Annual Review*
749 *of Ecology, Evolution, and Systematics* **47**, 507–532 (2016).

750 6. R. Butlin, *et al.*, What do we need to know about speciation? *Trends in Ecology and*
751 *Evolution* **27**, 27–39 (2012).

752 7. J. A. Coyne, H. A. Orr, *Speciation* (Oxford University Press, 2004).

753 8. D. R. Matute, B. S. Cooper, Comparative studies on speciation: 30 years since Coyne and
754 Orr. *Evolution* **75**, 764–778 (2021).

755 9. D. Schluter, L. H. Rieseberg, Three problems in the genetics of speciation by selection.
756 *Proceedings of the National Academy of Sciences* **119**, e2122153119 (2022).

757 10. D. Berner, W. Salzburger, The genomics of organismal diversification illuminated by
758 adaptive radiations. *Trends in Genetics* **31**, 491–499 (2015).

759 11. D. A. Marques, J. I. Meier, O. Seehausen, A Combinatorial View on Speciation and
760 Adaptive Radiation. *Trends in Ecology & Evolution* **34**, 531–544 (2019).

761 12. J. B. Pease, D. C. Haak, M. W. Hahn, L. C. Moyle, Phylogenomics Reveals Three Sources
762 of Adaptive Variation during a Rapid Radiation. *PLOS Biology* **14**, e1002379 (2016).

763 13. B. W. Stone, C. A. Wessinger, Ecological Diversification in an Adaptive Radiation of
764 Plants: The Role of De Novo Mutation and Introgression. *Mol Biol Evol* **41**, msae007
765 (2024).

766 14. R. D. H. Barrett, D. Schluter, Adaptation from standing genetic variation. *Trends in*
767 *Ecology & Evolution* **23**, 38–44 (2008).

768 15. M. Rousselle, *et al.*, Is adaptation limited by mutation? A timescale-dependent effect of
769 genetic diversity on the adaptive substitution rate in animals. *PLOS Genetics* **16**, e1008668
770 (2020).

771 16. O. Seehausen, Hybridization and adaptive radiation. *Trends in Ecology & Evolution* **19**,
772 198–207 (2004).

773 17. K. Kagawa, G. Takimoto, O. Seehausen, Transgressive segregation in mating traits drives
774 hybrid speciation. *Evolution* **77**, 1622–1633 (2023).

775 18. K. Kagawa, G. Takimoto, Hybridization can promote adaptive radiation by means of
776 transgressive segregation. *Ecology Letters* **21**, 264–274 (2018).

19. R. De-Kayne, *et al.*, Genomic architecture of adaptive radiation and hybridization in Alpine whitefish. *Nat Commun* **13**, 4479 (2022).

20. D. A. Joyce, *et al.*, Repeated colonization and hybridization in Lake Malawi cichlids. *Current Biology* **21**, R108–R109 (2011).

21. S. Lamichhaney, *et al.*, Evolution of Darwin's finches and their beaks revealed by genome sequencing. *Nature* **518**, 371–375 (2015).

22. C. H. Martin, *et al.*, Complex histories of repeated gene flow in Cameroon crater lake cichlids cast doubt on one of the clearest examples of sympatric speciation. *Evol* **69**, 1406–1422 (2015).

23. J. I. Meier, *et al.*, Ancient hybridization fuels rapid cichlid fish adaptive radiations. *Nat Commun* **8**, 14363 (2017).

24. C. Pouchon, *et al.*, Phylogenomic Analysis of the Explosive Adaptive Radiation of the Espeletia Complex (Asteraceae) in the Tropical Andes. *Syst Biol* **67**, 1041–1060 (2018).

25. E. J. Richards, J. W. Poelstra, C. H. Martin, Don't throw out the sympatric speciation with the crater lake water: fine-scale investigation of introgression provides equivocal support for causal role of secondary gene flow in one of the clearest examples of sympatric speciation. *Evolution Letters* **2**, 524–540 (2018).

26. E. J. Richards, *et al.*, A vertebrate adaptive radiation is assembled from an ancient and disjunct spatiotemporal landscape. *Proceedings of the National Academy of Sciences* **118**, e2011811118 (2021).

27. N. Rosser, *et al.*, Hybrid speciation driven by multilocus introgression of ecological traits. *Nature* **628**, 811–817 (2024).

28. M. E. S. John, J. C. Dunker, E. J. Richards, S. Romero, C. H. Martin, Parallel genetic changes underlie integrated craniofacial traits in an adaptive radiation of trophic specialist pupfishes. [Preprint] (2021). Available at: https://www.biorxiv.org/content/10.1101/2021.07.01.450661v2 [Accessed 21 November 2023].

29. C. H. Martin, P. C. Wainwright, Trophic novelty is linked to exceptional rates of morphological diversification in two adaptive radiations of cyprinodon pupfish. *Evolution* **65**, 2197–2212 (2011).

30. A. H. Patton, E. J. Richards, K. J. Gould, L. K. Buie, C. H. Martin, Hybridization alters the shape of the genotypic fitness landscape, increasing access to novel fitness peaks during adaptive radiation. *eLife* **11**, e72905 (2022).

31. E. J. Richards, C. H. Martin, Adaptive introgression from distant Caribbean islands contributed to the diversification of a microendemic adaptive radiation of trophic specialist pupfishes. *PLOS Genetics* **13**, e1006919 (2017).

32. E. J. Richards, C. H. Martin, We get by with a little help from our friends: shared adaptive variation provides a bridge to novel ecological specialists during adaptive radiation. *Proc Biol Sci* **289**, 20220613 (2022).

33. J. M. Humphries, R. R. Miller, A Remarkable Species Flock of Pupfishes, Genus Cyprinodon, from Yucatán, México. *Copeia* **1981**, 52–64 (1981).

34. D. A. Hodell, J. H. Curtis, M. Brenner, Possible role of climate in the collapse of Classic Maya civilization. *Nature* **375**, 391–394 (1995).

35. U. Strecker, Description of a new species from Laguna Chichancanab, Yucatan, Mexico: Cyprinodon suavium (Pisces: Cyprinodontidae). *Hydrobiologia* **541**, 107–115 (2005).

36. J. M. Humphries, Cyprinodon verecundus, n. sp., a Fifth Species of Pupfish from Laguna Chichancanab. *Copeia* **1984**, 58–68 (1984).

37. C. A. Gracida-Juárez, J. J. Schmitter-Soto, M. J. Genner, Community structure of indigenous fishes relative to habitat variation and invasive tilapia in lakes of Quintana Roo, Mexico. *Environmental Biology of Fishes* **107**, 401–414 (2024).

38. U. Strecker, The impact of invasive fish on an endemic Cyprinodon species flock (Teleostei) from Laguna Chichancanab, Yucatan, Mexico. *Ecology of Freshwater Fish* **15**, 408–418 (2006).

39. U. Strecker, Genetic differentiation and reproductive isolation in a *Cyprinodon* fish species flock from Laguna Chichancanab, Mexico. *Molecular Phylogenetics and Evolution* **39**, 865–872 (2006).

40. U. Strecker, C. G. Meyer, C. Sturmbauer, H. Wilkens, Genetic Divergence and Speciation in an Extremely Young Species Flock in Mexico Formed by the Genus*Cyprinodon*(Cyprinodontidae, Teleostei). *Molecular Phylogenetics and Evolution* **6**, 143–149 (1996).

41. M. Shpak, K. N. Lawrence, J. E. Pool, The Precision and Power of Population Branch Statistics in Identifying the Genomic Signatures of Local Adaptation. *Genome Biol Evol* **17**, evaf080 (2025).

42. J. A. McGirr, C. H. Martin, Novel Candidate Genes Underlying Extreme Trophic Specialization in Caribbean Pupfishes. *Molecular Biology and Evolution* **34**, 873 (2017).

43. J. A. McGirr, C. H. Martin, Parallel evolution of gene expression between trophic specialists despite divergent genotypes and morphologies. *Evol Lett* **2**, 62–75 (2018).

44. J. A. McGirr, C. H. Martin, Ecological divergence in sympatry causes gene misexpression in hybrids. *Molecular Ecology* **29**, 2707–2721 (2020).

45. J. A. McGirr, C. H. Martin, Few Fixed Variants between Trophic Specialist Pupfish Species Reveal Candidate Cis-Regulatory Alleles Underlying Rapid Craniofacial Divergence. *Mol Biol Evol* **38**, 405–423 (2021).

46. M. F. Palominos, V. Muhl, C. H. Martin, Craniofacial-specific transcriptomics uncovers novel genes underlying jaw divergence in dietary specialist pupfishes. *Genetics* iyaf207 (2025). https://doi.org/10.1093/genetics/iyaf207.

47. C. Bragato, *et al.*, Zebrafish dnm1a gene plays a role in the formation of axons and synapses in the nervous tissue. *Journal of Neuroscience Research* **101**, 1345–1359 (2023).

48. C. Gonzaga-Jauregui, *et al.*, Exome Sequence Analysis Suggests that Genetic Burden Contributes to Phenotypic Variability and Complex Neuropathy. *Cell Reports* **12**, 1169–1183 (2015).

49. M. Malinsky, M. Matschiner, H. Svardal, Dsuite - Fast D-statistics and related admixture evidence from VCF files. *Molecular Ecology Resources* **21**, 584–595 (2021).

50. B. Pfeifer, D. D. Kapan, Estimates of introgression as a function of pairwise distances. *BMC Bioinformatics* **20**, 207 (2019).

51. J. Smith, G. Coop, M. Stephens, J. Novembre, Estimating Time to the Common Ancestor for a Beneficial Allele. *Mol Biol Evol* **35**, 1003–1017 (2018).

52. J. T. Streelman, P. D. Danley, The stages of vertebrate evolutionary radiation. *Trends in Ecology & Evolution* **18**, 126–131 (2003).

53. W.-G. Li, T.-L. Xu, ASIC3 Channels in Multimodal Sensory Perception. *ACS Chem. Neurosci.* **2**, 26–37 (2011).

54. T. Le, *et al.*, A zebrafish model of crim1 loss of function has small and misshapen lenses with dysregulated clic4 and fgf1b expression. *Front. Cell Dev. Biol.* **13** (2025).

55. B. N. Kennedy, *et al.*, Zebrafish *rx3* and *mab21l2* are required during eye morphogenesis. *Developmental Biology* **270**, 336–349 (2004).

56. S. C. F. Neuhauss, *et al.*, Genetic Disorders of Vision Revealed by a Behavioral Screen of 400 Essential Loci in Zebrafish. *J. Neurosci.* **19**, 8603–8615 (1999).

57. M. H. K. Chau, *et al.*, Investigation of the genetic etiology in male infertility with apparently balanced chromosomal structural rearrangements by genome sequencing. *Asian Journal of Andrology* **24** (2022).

58. H. Li, Y. Dai, Z. Luo, D. Nie, Cloning of a new testis-enriched gene C4orf22 and its role in cell cycle and apoptosis in mouse spermatogenic cells. *Mol Biol Rep* **46**, 2029–2038 (2019).

879 59. Y. Miyamoto, *et al.*, The STK35 locus contributes to normal gametogenesis and encodes a
880 lncRNA responsive to oxidative stress. *Biol Open* **7**, bio032631 (2018).

881 60. S. Nawaz, S. Hussain, S. Basit, W. Ahmad, First evidence of involvement of *TBC1D25* in
882 causing human male infertility. *European Journal of Medical Genetics* **64**, 104142 (2021).

883 61. T. A. Square, *et al.*, Modulation of tooth regeneration through opposing responses to Wnt
884 and BMP signals in teleosts. *Development* **150**, dev202168 (2023).

885 62. S. Nawaz, *et al.*, WNT10A missense mutation associated with a complete Odonto-
886 Onycho-Dermal Dysplasia syndrome. *Eur J Hum Genet* **17**, 1600–1605 (2009).

887 63. E. L. Benard, *et al.*, wnt10a is required for zebrafish median fin fold maintenance and
888 adult unpaired fin metamorphosis. *Developmental Dynamics* **253**, 566–592 (2024).

889 64. J. L. Catrow, Y. Zhang, M. Zhang, H. Ji, Discovery of Selective Small-Molecule Inhibitors
890 for the β-Catenin/T-Cell Factor Protein–Protein Interaction through the Optimization of
891 the Acyl Hydrazone Moiety. *J. Med. Chem.* **58**, 4678–4692 (2015).

892 65. F. C. Gonsalves, *et al.*, An RNAi-based chemical genetic screen identifies three small-
893 molecule inhibitors of the Wnt/wingless signaling pathway. *Proceedings of the National*
894 *Academy of Sciences* **108**, 5954–5963 (2011).

895 66. E. D. Enbody, *et al.*, Community-wide genome sequencing reveals 30 years of Darwin's
896 finch evolution. *Science* **381**, eadf6218 (2023).

897 67. J. V. Peñalba, *et al.*, The Role of Hybridization in Species Formation and Persistence. *Cold*
898 *Spring Harb Perspect Biol* **16**, a041445 (2024).

899 68. O. Seehausen, Conditions when hybridization might predispose populations for adaptive
900 radiation. *Journal of Evolutionary Biology* **26**, 279–281 (2013).

901 69. D. Schluter, ADAPTIVE RADIATION ALONG GENETIC LINES OF LEAST
902 RESISTANCE. *Evol* **50**, 1766–1774 (1996).

903 70. T. Hornemann, *et al.*, The SPTLC3 Subunit of Serine Palmitoyltransferase Generates
904 Short Chain Sphingoid Bases *. *Journal of Biological Chemistry* **284**, 26322–26330
905 (2009).

906 71. M. E. Bronner, N. M. LeDouarin, Development and evolution of the neural crest: An
907 overview. *Developmental Biology* **366**, 2–9 (2012).

908 72. F. Hirth, H. Reichert, Conserved genetic programs in insect and mammalian brain
909 development. *BioEssays* **21**, 677–684 (1999).

910 73. C. J. Reaume, M. B. Sokolowski, Conservation of gene function in behaviour.
911 *Philosophical Transactions of the Royal Society B: Biological Sciences* **366**, 2100–2110
912 (2011).

74. A. Abzhanov, M. Protas, B. R. Grant, P. R. Grant, C. J. Tabin, Bmp4 and Morphological Variation of Beaks in Darwin's Finches. *Science* **305**, 1462–1465 (2004).

75. R. C. Albertson, J. T. Streelman, T. D. Kocher, P. C. Yelick, Integration and evolution of the cichlid mandible: The molecular basis of alternate feeding strategies. *Proceedings of the National Academy of Sciences* **102**, 16287–16292 (2005).

76. Y. Terai, N. Morikawa, N. Okada, The Evolution of the Pro-Domain of Bone Morphogenetic Protein 4 (Bmp4) in an Explosively Speciated Lineage of East African Cichlid Fishes. *Mol Biol Evol* **19**, 1628–1632 (2002).

77. K. L. Carleton, D. Escobar-Camacho, S. M. Stieb, F. Cortesi, N. J. Marshall, Seeing the rainbow: mechanisms underlying spectral sensitivity in teleost fishes. *J Exp Biol* **223**, jeb193334 (2020).

78. C. M. Hofmann, *et al.*, The Eyes Have It: Regulatory and Structural Changes Both Underlie Cichlid Visual Pigment Diversity. *PLOS Biology* **7**, e1000266 (2009).

79. K. E. O'Quin, C. M. Hofmann, H. A. Hofmann, K. L. Carleton, Parallel Evolution of Opsin Gene Expression in African Cichlid Fishes. *Mol Biol Evol* **27**, 2839–2854 (2010).

80. M. G. Ritchie, Sexual Selection and Speciation. *Annual Review of Ecology, Evolution, and Systematics* **38**, 79–102 (2007).

81. M. R. Servedio, J. W. Boughman, The Role of Sexual Selection in Local Adaptation and Speciation. *Annual Review of Ecology, Evolution, and Systematics* **48**, 85–109 (2017).

82. A. Devigili, *et al.*, Possible glimpses into early speciation: the effect of ovarian fluid on sperm velocity accords with post-copulatory isolation between two guppy populations. *Journal of Evolutionary Biology* **31**, 66–74 (2018).

83. M. D. Garlovsky, *et al.*, Synthesis and Scope of the Role of Postmating Prezygotic Isolation in Speciation. *Cold Spring Harb Perspect Biol* a041429 (2023). https://doi.org/10.1101/cshperspect.a041429.

84. M. C. Kustra, M. R. Servedio, S. H. Alonzo, Cryptic female choice can maintain reproductive isolation. *Evol* **79**, 2259–2273 (2025).

85. M. C. Kustra, S. H. Alonzo, The coevolutionary dynamics of cryptic female choice. *Evolution Letters* **7**, 191–202 (2023).

86. P. D. Lorch, M. R. Servedio, The evolution of conspecific gamete precedence and its effect on reinforcement. *Journal of Evolutionary Biology* **20**, 937–949 (2007).

87. J. L. Marshall, M. L. Arnold, D. J. Howard, Reinforcement: the road not taken. *Trends in Ecology & Evolution* **17**, 558–563 (2002).

88. A. Kodric-Brown, R. J. D. West, Asymmetries in premating isolating mechanisms in a sympatric species flock of pupfish (Cyprinodon). *Behavioral Ecology* **25**, 69–75 (2014).

89. U. Strecker, A. Kodric-Brown, Mate recognition systems in a species flock of Mexican pupfish. *Journal of Evolutionary Biology* **12**, 927–935 (1999).

90. L. Campagna, *et al.*, Repeated divergent selection on pigmentation genes in a rapid finch radiation. *Science Advances* **3**, e1602404 (2017).

91. F. C. Jones, *et al.*, The genomic basis of adaptive evolution in threespine sticklebacks. *Nature* **484**, 55–61 (2012).

92. Z. D. Blount, R. E. Lenski, J. B. Losos, Contingency and determinism in evolution: Replaying life's tape. *Science* **362**, eaam5979 (2018).

93. P. W. Hedrick, Adaptive introgression in animals: examples and comparison to new mutation and standing variation as sources of adaptive variation. *Molecular Ecology* **22**, 4606–4618 (2013).

94. S. G. Das, M. Mungan, J. Krug, Epistasis-mediated compensatory evolution in a fitness landscape with adaptational tradeoffs. *Proceedings of the National Academy of Sciences* **122**, e2422520122 (2025).

95. M. J. Harms, J. W. Thornton, Historical contingency and its biophysical basis in glucocorticoid receptor evolution. *Nature* **512**, 203–207 (2014).

96. M. Karageorgi, *et al.*, Genome editing retraces the evolution of toxin resistance in the monarch butterfly. *Nature* **574**, 409–412 (2019).

97. R. D. Tarvin, *et al.*, Interacting amino acid replacements allow poison frogs to evolve epibatidine resistance. *Science* **357**, 1261–1266 (2017).

98. D. M. Weinreich, N. F. Delaney, M. A. DePristo, D. L. Hartl, Darwinian Evolution Can Follow Only Very Few Mutational Paths to Fitter Proteins. *Science* **312**, 111–114 (2006).

99. S. Chen, Y. Zhou, Y. Chen, J. Gu, fastp: an ultra-fast all-in-one FASTQ preprocessor. *Bioinformatics* **34**, i884–i890 (2018).

100. H. Li, Aligning sequence reads, clone sequences and assembly contigs with BWA-MEM. [Preprint] (2013). Available at: http://arxiv.org/abs/1303.3997 [Accessed 22 September 2025].

101. K. Okonechnikov, A. Conesa, F. García-Alcalde, Qualimap 2: advanced multi-sample quality control for high-throughput sequencing data. *Bioinformatics* **32**, 292–294 (2016).

102. A. McKenna, *et al.*, The Genome Analysis Toolkit: A MapReduce framework for analyzing next-generation DNA sequencing data. *Genome Res.* **20**, 1297–1303 (2010).

979 103. M. A. DePristo, *et al.*, A framework for variation discovery and genotyping using next-
980 generation DNA sequencing data. *Nat Genet* **43**, 491–498 (2011).

981 104. G. A. Van der Auwera, *et al.*, From FastQ Data to High-Confidence Variant Calls: The
982 Genome Analysis Toolkit Best Practices Pipeline. *Current Protocols in Bioinformatics* **43**,
983 11.10.1-11.10.33 (2013).

984 105. D. Caetano-Anolles, GenotypeGVCFs and the death of the dot (obsolete as of GATK
985 4.6.0.0). *GATK* (2024). Available at: https://gatk.broadinstitute.org/hc/en-
986 us/articles/6012243429531-GenotypeGVCFs-and-the-death-of-the-dot-obsolete-as-of-
987 GATK-4-6-0-0 [Accessed 27 July 2025].

988 106. P. Danecek, *et al.*, Twelve years of SAMtools and BCFtools. *Gigascience* **10**, giab008
989 (2021).

990 107. S. Purcell, *et al.*, PLINK: A Tool Set for Whole-Genome Association and Population-
991 Based Linkage Analyses. *The American Journal of Human Genetics* **81**, 559–575 (2007).

992 108. D. H. Alexander, J. Novembre, K. Lange, Fast model-based estimation of ancestry in
993 unrelated individuals. *Genome Res.* **19**, 1655–1664 (2009).

994 109. S. Schiffels, K. Wang, "MSMC and MSMC2: The Multiple Sequentially Markovian
995 Coalescent" in *Statistical Population Genomics*, J. Y. Dutheil, Ed. (Springer US, 2020),
996 pp. 147–166.

997 110. P. Danecek, *et al.*, The variant call format and VCFtools. *Bioinformatics* **27**, 2156–2158
998 (2011).

999 111. J. M. Schmidt, M. de Manuel, T. Marques-Bonet, S. Castellano, A. M. Andrés, The impact
1000 of genetic adaptation on chimpanzee subspecies differentiation. *PLOS Genetics* **15**,
1001 e1008485 (2019).

1002 112. S. G. Hernández-Ávila, C. W. Hoagstrom, W. A. Matamoros, Historical biogeography of
1003 North American killifishes (Cyprinodontiformes) recapitulates geographical history in the
1004 Gulf of México watershed. *Zool J Linn Soc* **202**, zlae105 (2024).

1005 113. E. Y. Durand, N. Patterson, D. Reich, M. Slatkin, Testing for Ancient Admixture between
1006 Closely Related Populations. *Mol Biol Evol* **28**, 2239–2252 (2011).

1007 114. C. Feng, J. Wang, A. Liston, M. Kang, Recombination Variation Shapes Phylogeny and
1008 Introgression in Wild Diploid Strawberries. *Mol Biol Evol* **40**, msad049 (2023).

1009 115. A. Morales-Cruz, *et al.*, Introgression among North American wild grapes (Vitis) fuels
1010 biotic and abiotic adaptation. *Genome Biology* **22**, 254 (2021).

1011 116. A. R. Quinlan, I. M. Hall, BEDTools: a flexible suite of utilities for comparing genomic
1012 features. *Bioinformatics* **26**, 841–842 (2010).

117. P. Cingolani, *et al.*, A program for annotating and predicting the effects of single nucleotide polymorphisms, SnpEff: SNPs in the genome of Drosophila melanogaster strain w1118; iso-2; iso-3. *Fly* **6**, 80–92 (2012).

118. M. Schumer, *et al.*, Natural selection interacts with recombination to shape the evolution of hybrid genomes. *Science* **360**, 656–660 (2018).

119. C. T. Rueden, *et al.*, ImageJ2: ImageJ for the next generation of scientific image data. *BMC Bioinformatics* **18**, 529 (2017).

120. D. Bates, M. Mächler, B. Bolker, S. Walker, Fitting Linear Mixed-Effects Models Using lme4. *Journal of Statistical Software* **67**, 1–48 (2015).

121. R. V. Lenth, *emmeans: Estimated Marginal Means, aka Least-Squares Means* (2021).

122. M. Walker, C. Kimmel, A two-color acid-free cartilage and bone stain for zebrafish larvae. *Biotechnic & Histochemistry* **82**, 23–28 (2007).

123. R. Koita, S. Oikawa, T. Tani, M. Matsuda, A. Kawamura, Live Visualization of Calcified Bones in Zebrafish and Medaka Larvae and Juveniles Using Calcein and Alizarin Red S. *Bio-protocol* **14** (2024).

124. R. Maier, *et al.*, On the limits of fitting complex models of population history to f-statistics. *eLife* **12**, e85492 (2023).

1043 **Supplementary materials**

1044

1045 **Table S1.** Mean genome-wide pairwise F_{ST} statistics within the Chichancanab radiation and with
1046 sister outgroup (*artifrons*).

	labiosus	***beltrani***	***artifrons***
simus	0.090	0.068	0.182
labiosus		0.032	0.184
beltrani			0.168

1047

1048 **Table S2.** F_{ST} statistics within the Chichancanab radiation.

Comparison	**F_{ST} = 1 (fixed)**	**1> F_{ST} ≥ 0.95 (nearly fixed)**	**0.95> F_{ST} ≥ 0.9**	**0.9> F_{ST} ≥0.8**	**Other**	**Mean F_{ST}**
simus vs beltrani + *labiosus*	19	1127	3304	20173	10359605	0.07
labiosus vs *beltrani* + *simus*	0	0	3	94	10384131	0.04
beltrani vs *simus* + *labiosus*	0	0	0	13	10384215	0.02

1049

1050

1051

1052

1053

1054

1055

1056

1057

1058

1059

1060

1061

1062 **Table S3.** Fixed SNPs between *C. simus* and *C. beltrani* + *C. labiosus*. Bold rows indicate SNPs within top 1% of PBS windows.

1063 Bolded genes only are genes that have regions that fall within the top 1% PBS percentile.

Position	Gene	Distance to gene	PBS percentile	Annotation
Chr 1: 5290600	**STK35**	12594	1.85	
Chr 1:5290602	**STK35**	12592	1.85	Fertility, eye development and oxidative stress (Miyamoto et al 2018).
Chr 1:5290604	**STK35**	12590	1.85	
Chr 2: 17498913	SLC17A8	Intron	1.24	Glutamate neurotransmitter, inner hair cell dysfunction
Chr 3: **11687002**	**AGO3**	**Intron**	**0.34**	**RNA regulator**
Chr 3: 32286614	RBMS3	14363	22.93	
Chr 3: 32286627	RBMS3	14350	22.93	Involved in chondrogenic craniofacial development of zebrafish
Chr 3: 32286638	RBMS3	14339	22.93	(Jayasena and Bronner 2012).
Chr 3: 32286614	RBMS3	14363	22.93	
Chr 11: 27324192	GRIA3	Intron	2.85	
Chr 11: 27336469	GRIA3	2772	3.18	Glutamate receptor strongly expressed in zebrafish retina
Chr 11: 27336472	GRIA3	2775	3.18	development.
Chr 11: 27336476	GRIA3	2779	3.18	
Chr 11: **28255536**	**NA**	**3026**	**0.98**	**NA**
Chr 11: **28255616**	**NA**	**3106**	**0.98**	**NA**
Chr 11: **28256343**	**NA**	**3833**	**0.98**	**NA**
Chr 11: **28257367**	**NA**	**4857**	**0.98**	**NA**
Chr 11: 28260047	NA	7537	2.87	NA
Chr 12: 13854139	**C4orf22**	11903	1.30	Spermatogenesis, cilia, flagellum
Chr 24: **12693158**	**KDM6A**	**Intron**	**0.05**	**Kabuki syndrome (craniofacial development)**

1064

1065 **Table S4.** Summary statistics of the distance between closest adaptive candidate SNPs within the same
1066 gene

Gene	Median Distance	Mean Distance	SD	
TM6SF2	7430	7430	NA	2
C19orf10	4789	4789	NA	2
KDM6A	2892.5	2892.5	2410.52702	3
KCNB2	1803	1738.75	1614.92299	5
UBE2T	1742	1742	NA	2
TMEM230	1734	3039	3599.52427	4
ABCA1	1037.5	1097.5	959.375665	5
HAPLN4	974	1608.21739	9927.05273	24
GRIN2A	904	1270.6667	4273.38008	4
DPH1	608	1224.5	1999.25934	7
WNT10A	402	1442.17857	3986.39626	29
OPN1LW	386.5	359.5	225.229513	5
NIPSNAP3A	253	1451.71429	2819.19065	8
GALNT15	246.5	675.166667	3156.86746	13
SWS2	246	1381.25	2423.03892	5
STK35	217	793.366667	1992.8543	31
CRIM1	201	47.829268	2176.05381	42
PDYN	187	326.371429	355.925561	36
ADCYAP1R1	186.5	833	1304.35501	11
DNM1	186.5	459.708333	677.261781	25
DNM1	186.5	459.708333	677.261781	25
KCNH8	131.5	584.366667	1030.65532	31
TOP1	124	332.375	6687.63393	17
AGO3	115	357.625	552.097284	9
GMEB2	112	319.490196	2485.05809	52
GPNMB	57	57	77.781746	3
IGFBP4	26	2254	3880.67997	4
FAM83D	23	2523.66667	4347.74658	4
EXOSC3	17	17	NA	2
C4orf22	15	15	9.899495	3
TMEM106B	7	11.4	10.358571	6
THOC3	6	5.833333	3.600926	7
MID1	1	1	NA	2

1067

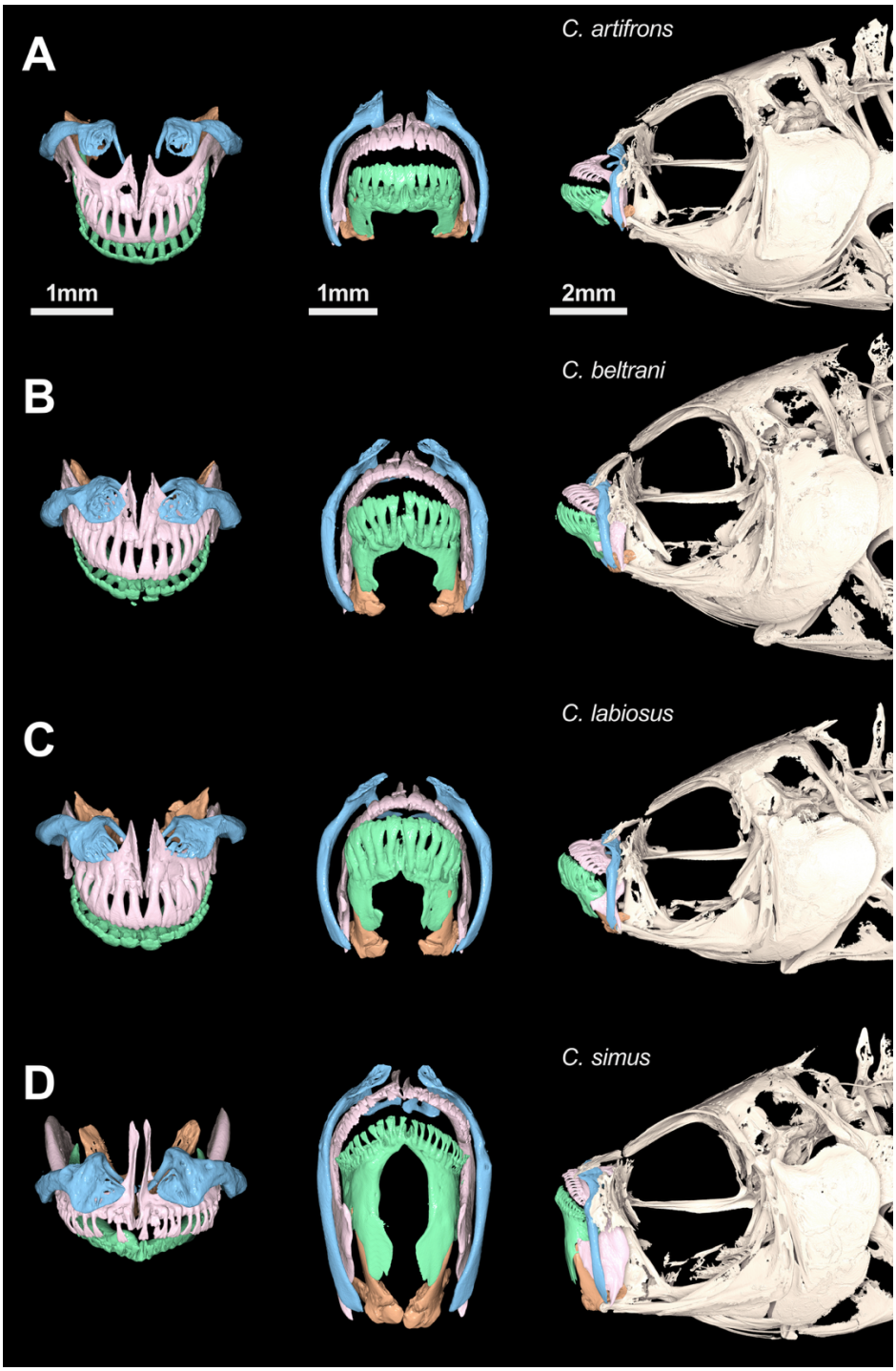

Figure S1. µCT scans of Yucatán pupfish with maxilla colored in blue, premaxilla in pink, dentary in green, and articular in orange.

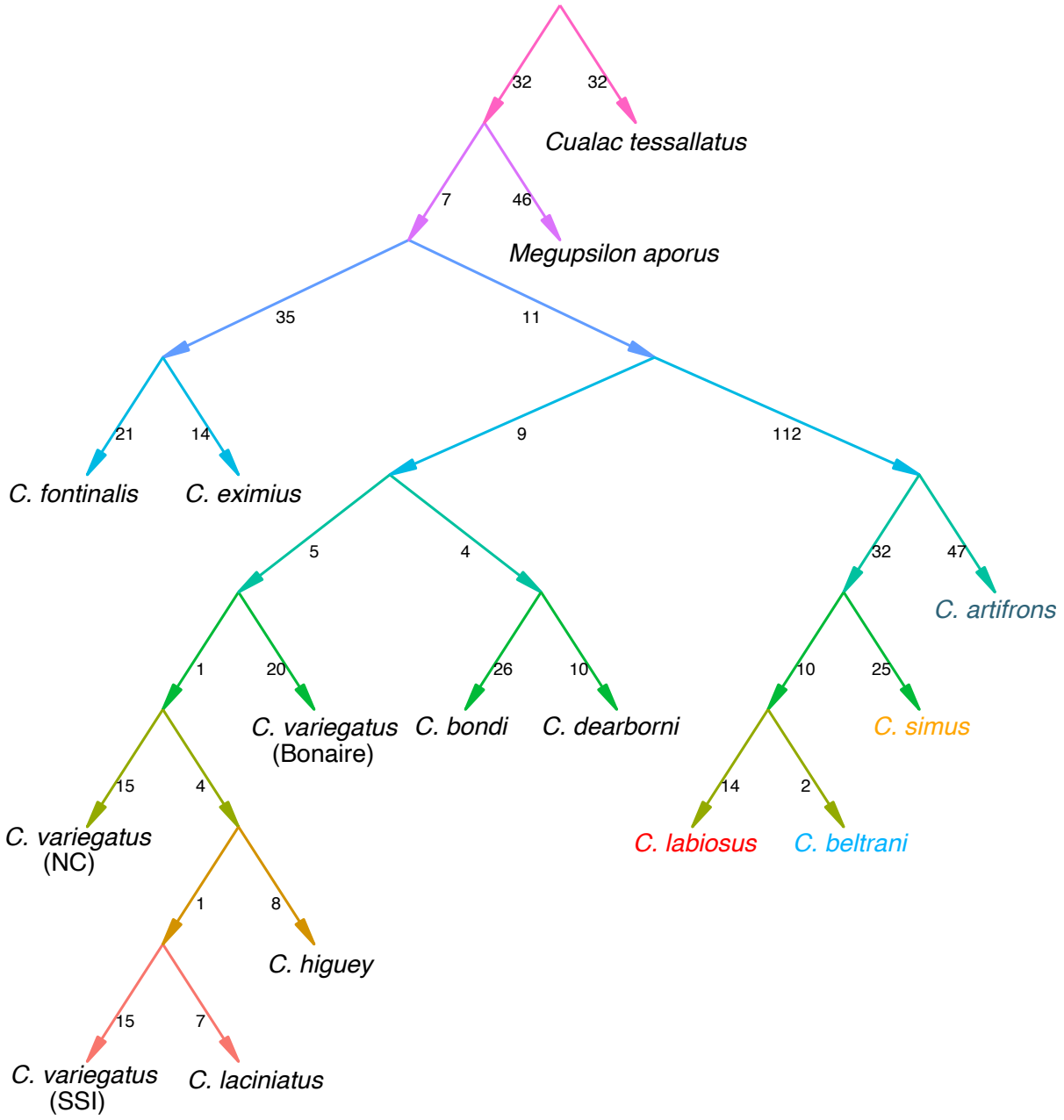

Figure S2. Best fitting admixture graph assuming zero admixture events. Admixture graph was found using the *findGraphs* function in *ADMIXTOOLS2* (124). Number on edges represent drift weights.

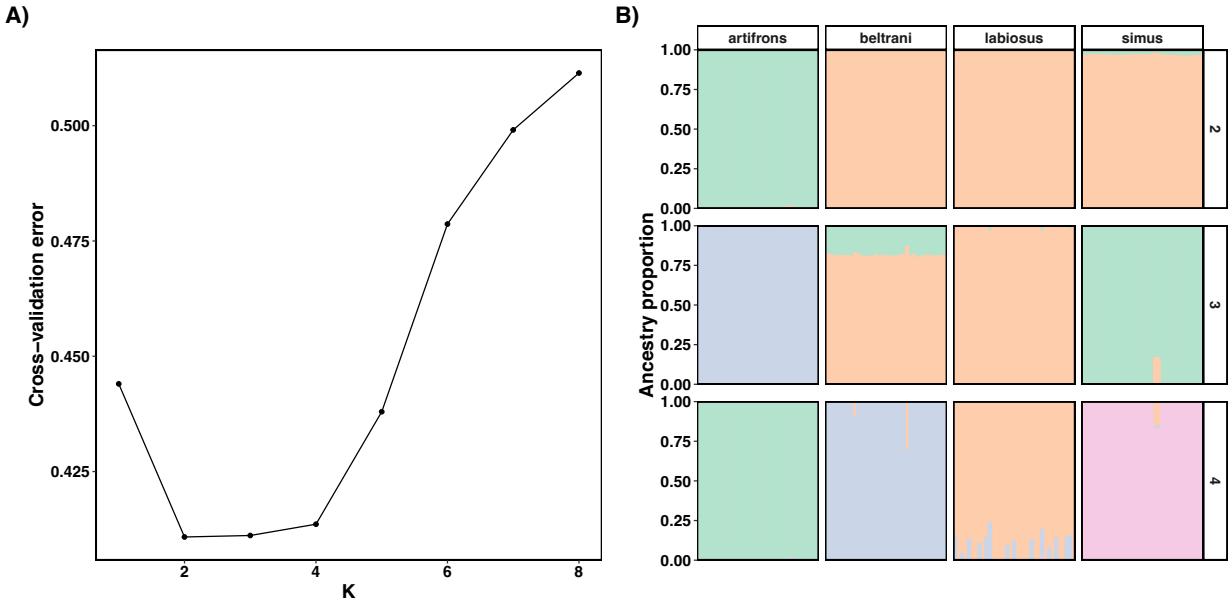

Figure S3. ADMIXTURE results support genetic differentiation of Yucatán Cyprinodon pupfish species. (A) Cross-validation error for different values of K clusters, equally support 2, 3, and 4 clusters. (B) ADMIXTURE plots showing the clusters at different values of K.

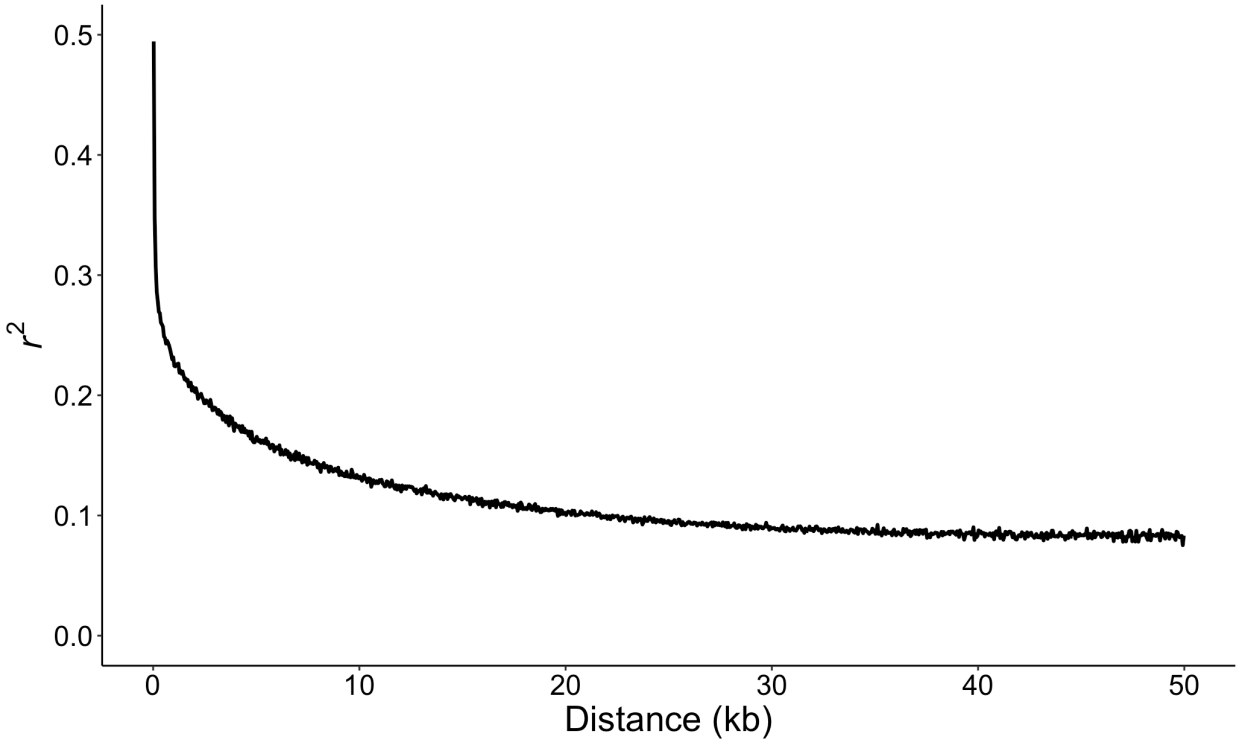

Figure S4. Linkage decay occurs rapidly in *Cyprinodon simus*. Linkage decay was calculated in windows of 1000KB using PLINK (v1.9). The results graphed are a random sample of all calculated r^2 values taken for plotting purposes (n = 9,645 r^2 values).

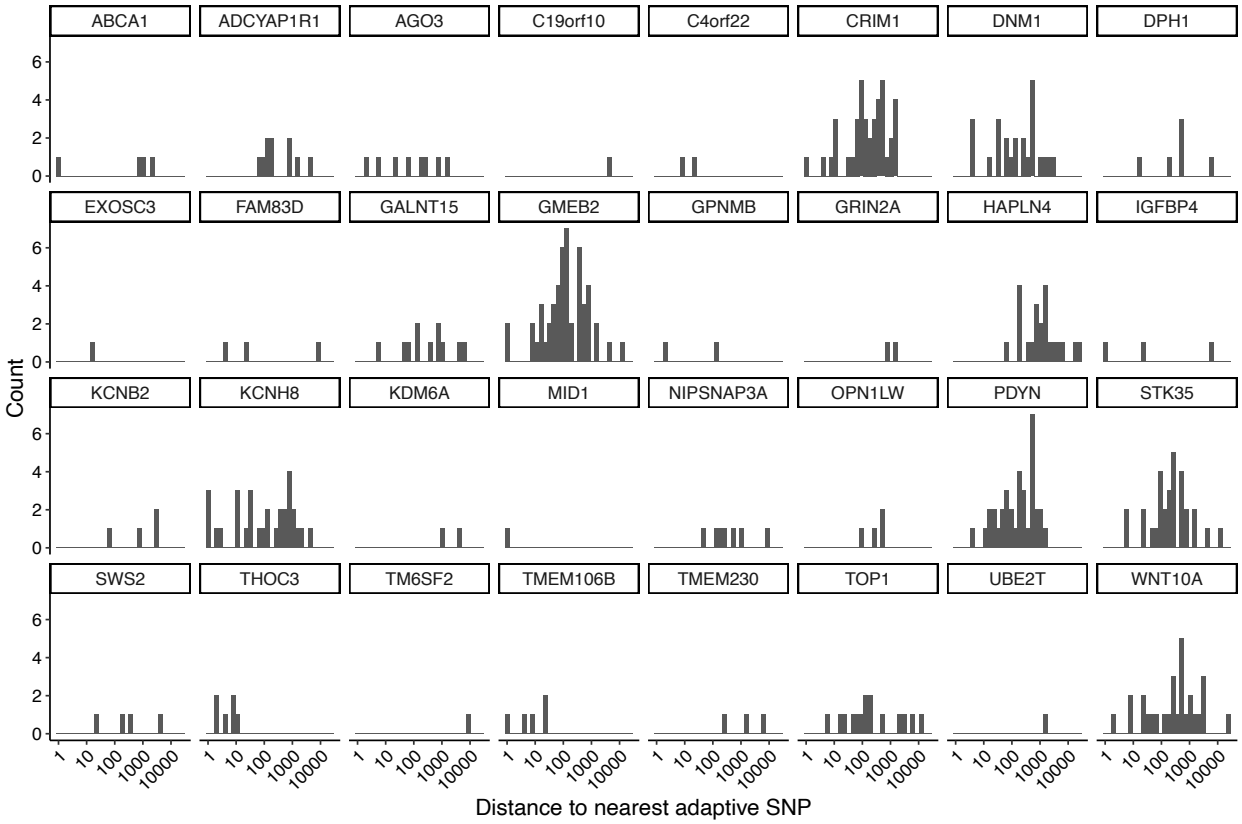

Figure S5. Adaptative SNPs associated with the same gene are generally spaced apart. Distribution of the distance to nearest adaptive SNP within a gene. Note the log scale of the x-axis.

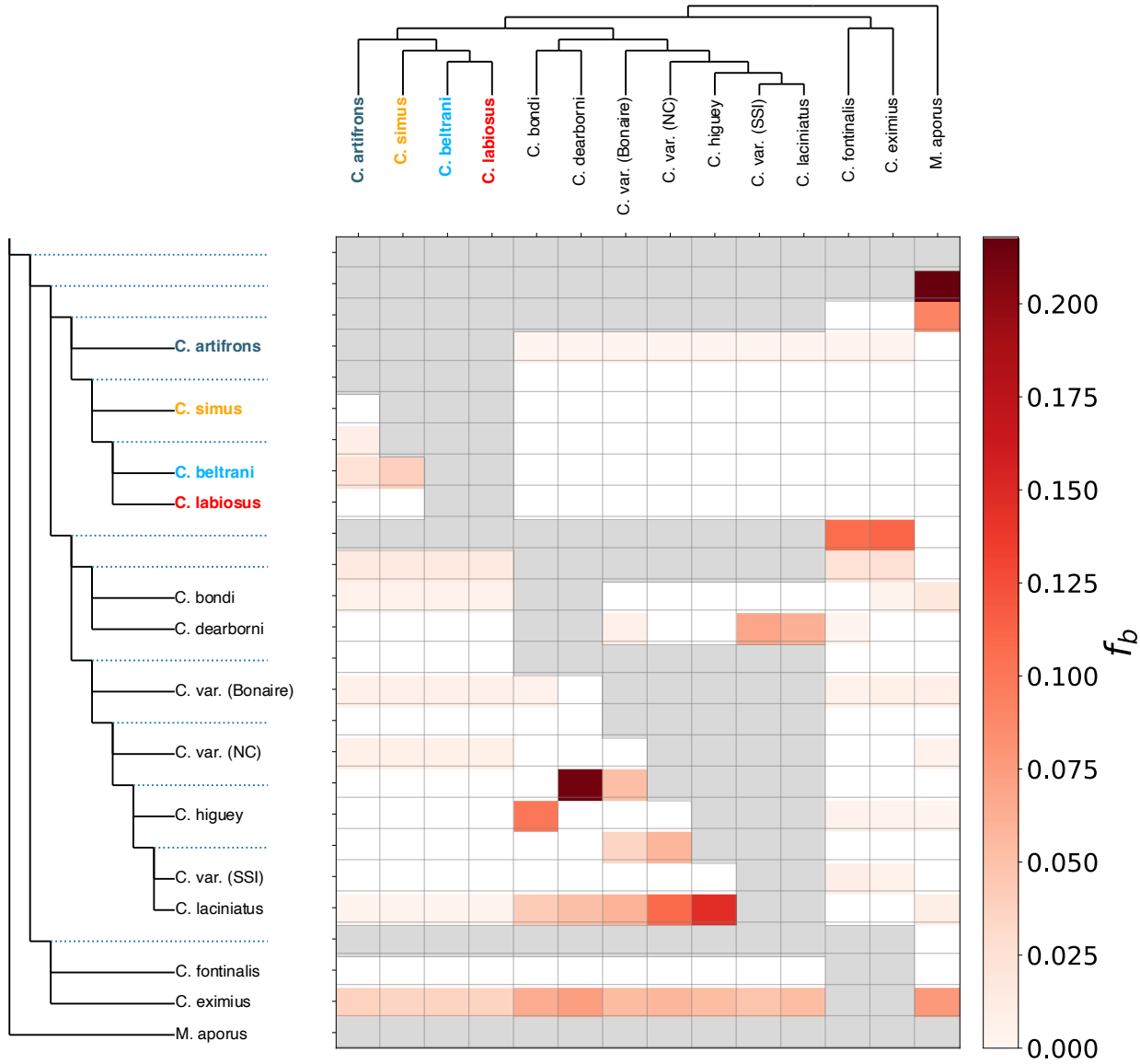

Figure S6. *f*-branch (f_b) show that introgression with desert pupfish occurred before the Chichancanab radiation. Boxes with red color represent significant introgression between P3 species (top) and the species/internal branch on the left. For visualization, non-significant f_b were changed to zero and are completely white boxes. Grey boxes represent comparisons that cannot be made, as f_b cannot be calculated for introgression between sister taxon. Dashed lines on the left are internal branches. SSI: San Salvador Island, Bahamas; NC: North Carolina, USA.

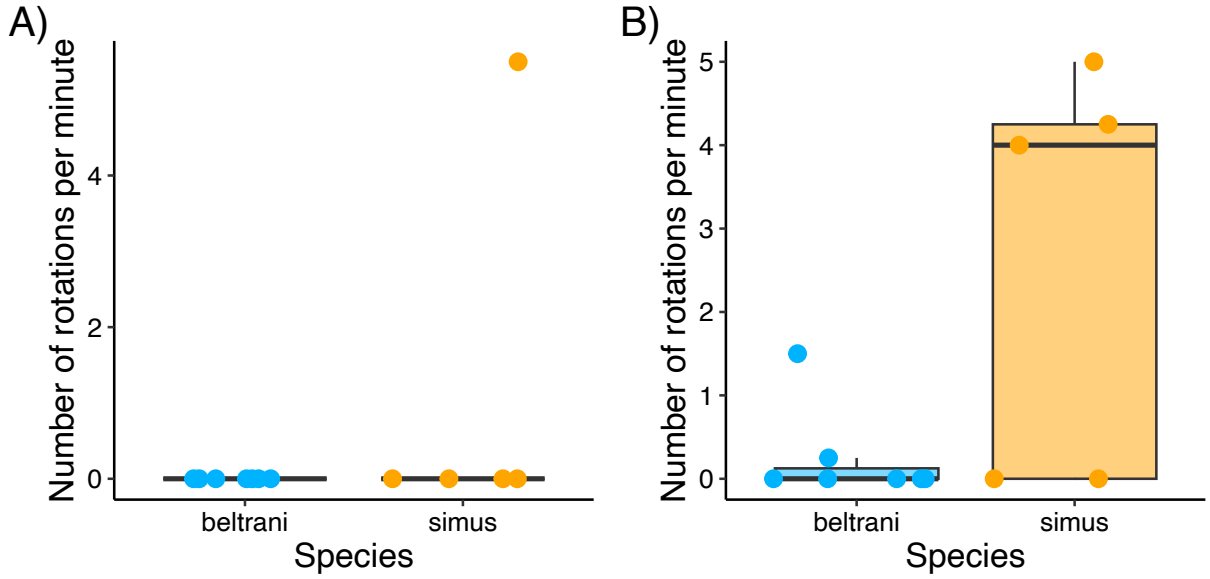

Figure S7. **Both species did not have a strong response to either control scenario in the optomotor response experiment. (A)** Number of complete rotations fish swam when the machine was off and **(B)** when the machine was on but the apparatus was all black**.** Boxplots and points of the number of complete rotations individuals performed during the "off-banded" portion of the experiment. Note that some boxplots are compressed to a single line because most individuals had no response.

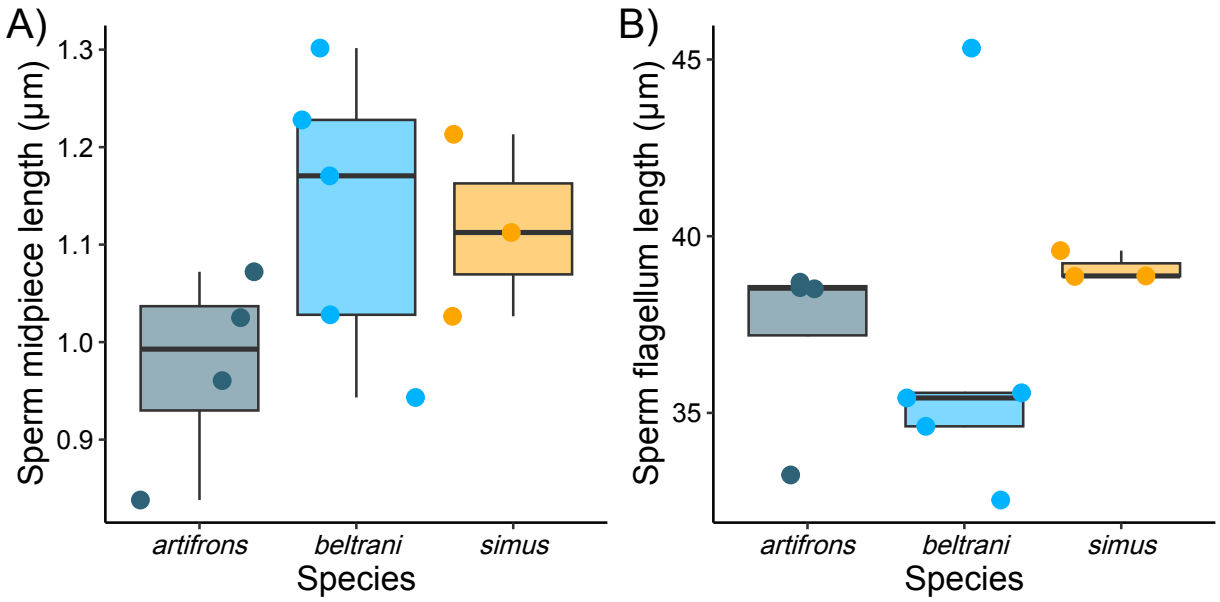

Figure S8. **Species do not differ in sperm midpiece size or sperm flagellum length.** Boxplots and points of the mean sperm morphological estimate for an individual.

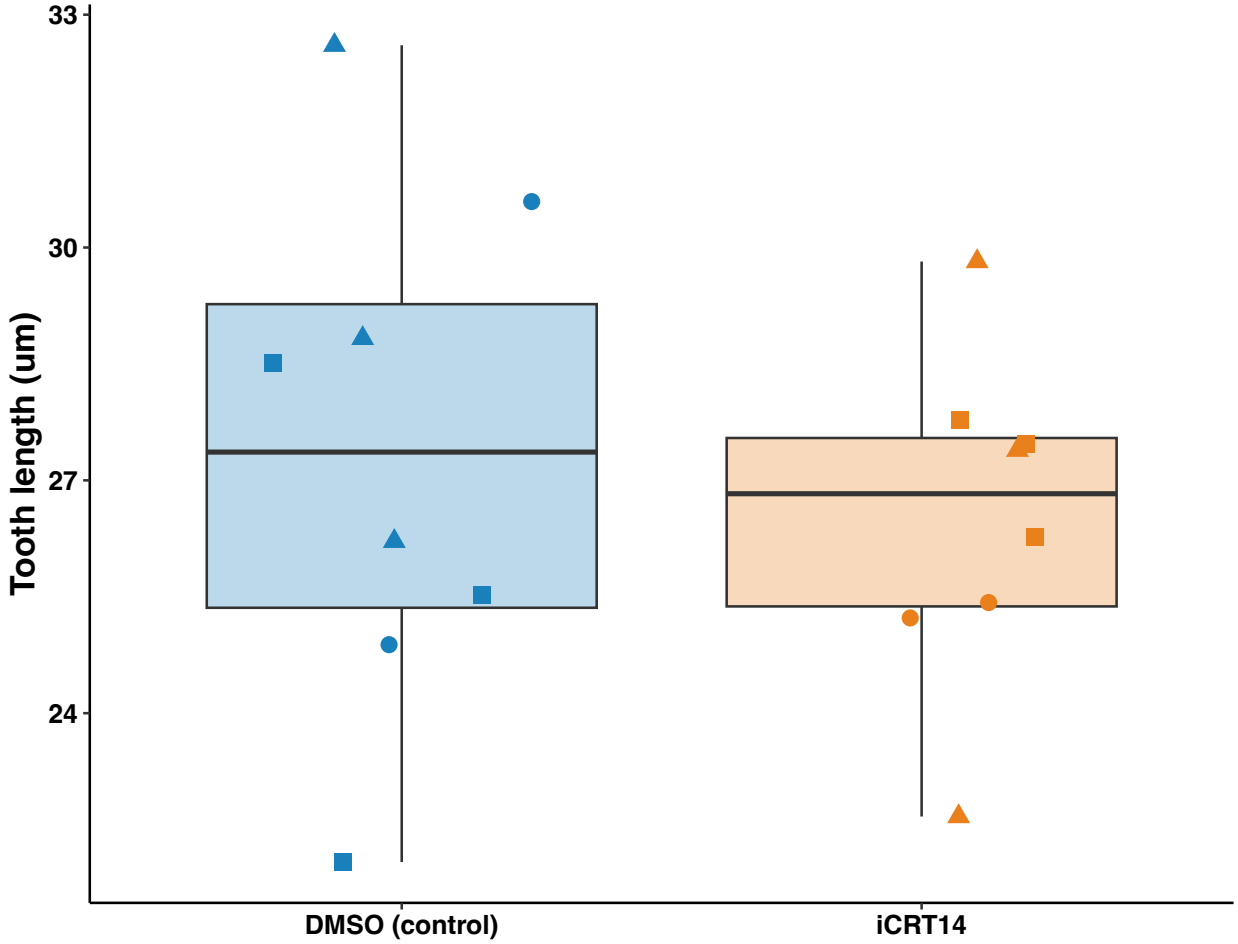

Figure S9. Tooth length was not affected by Wnt inhibition. Boxplot and jittered points of average tooth length of the left and right teeth closest to the mandibular symphysis for *C. beltrani* larvae treated with either a control or Wnt inhibitor (iCRT14). Shapes represent different split-brood replicates.

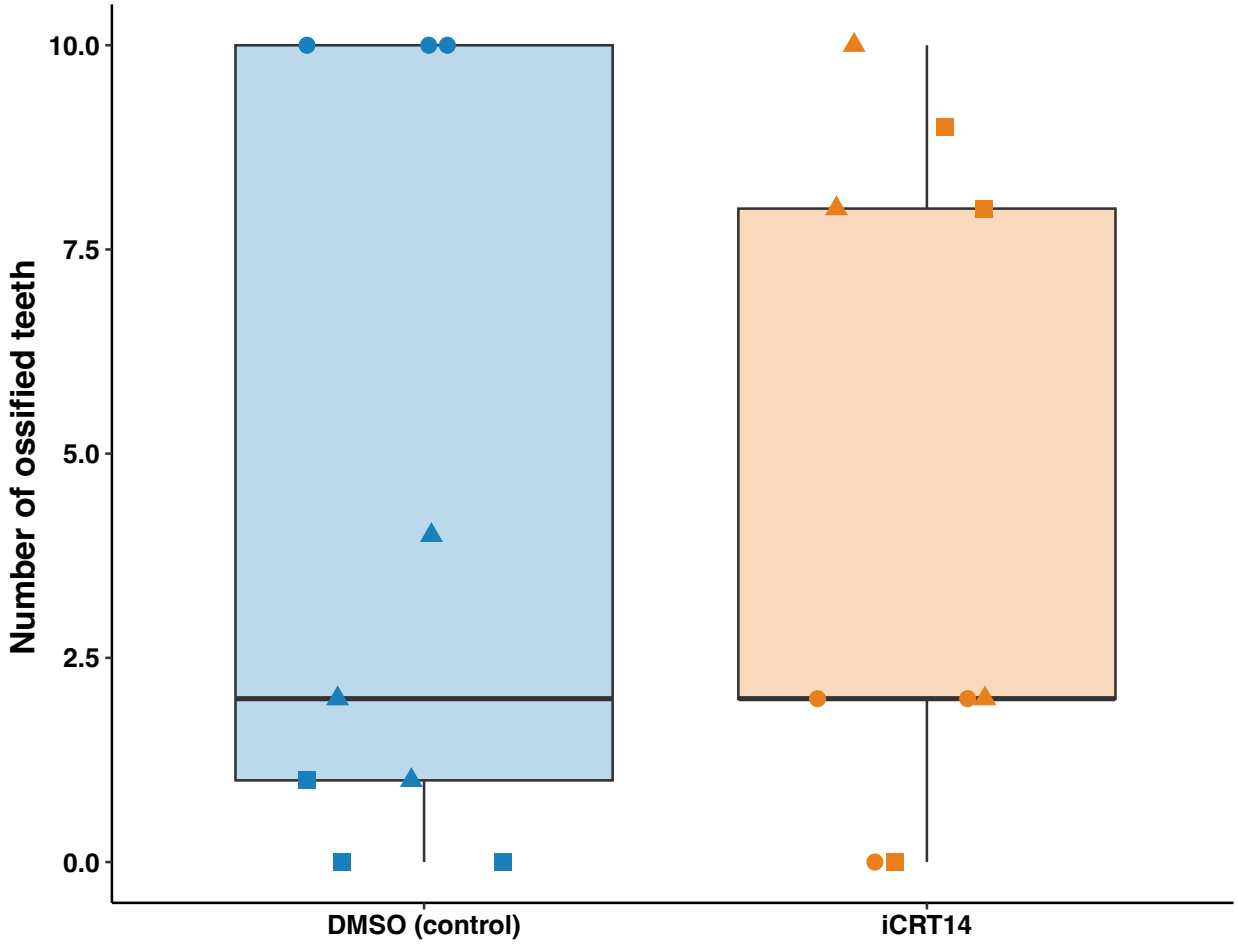

Figure S10. Number of ossified teeth was not affected by Wnt inhibition. Boxplot and jittered points of number of ossified teeth in *C. beltrani* larvae treated with either a control or Wnt inhibitor (iCRT14). Shapes represent different split-brood replicates.